2009

Electronic to Vibrational Energy Transfer from Cl^* ($^2P_{1/2}$) to CH_4 and CD_4

Brian R. Munson
Wright State University

ELECTRONIC TO VIBRATIONAL ENERGY TRANSFER FROM $Cl^*(^2P_{1/2})$ TO CH_4 and CD_4

A thesis submitted in partial fulfillment
of the requirements for the degree of
Master of Science

By

BRIAN R. MUNSON
B.S., Texas A&M University, 1997

2009
Wright State University

WRIGHT STATE UNIVERSITY

SCHOOL OF GRADUATE STUDIES

March 11, 2009

I HEREBY RECOMMEND THAT THE THESIS PEPARED UNDER MY SUPERVISION BY Brian R. Munson ENTITLED Electronic to Vibrational Energy Transfer from $Cl^*(^2P_{1/2})$ to CH_4 and CD_4 BE ACCEPTED IN PARTIAL FULFILLMENT OF THE REQUIREMENTS FOR THE DEGREE OF Master of Science.

David A. Dolson, Ph.D.
Thesis Director

Kenneth Turnbull, Ph.D.
Department Chair

Committee on
Final Examination

David A. Dolson, Ph.D.

Paul G. Seybold, Ph.D.

Steven R. Higgins, Ph.D.

Joseph F. Thomas, Jr., Ph.D.
Dean, School of Graduate Studies

ABSTRACT

Munson, Brian R. M.S., Department of Chemistry, Wright State University, 2009.
Electronic to Vibrational Energy Transfer from Cl^* ($^2P_{1/2}$) to CH_4 and CD_4.

.

Electronic-to-vibrational (E-V) energy transfer is a significant kinetic channel in the collisional quenching of spin-orbit excited chlorine atoms, Cl^* ($^2P_{1/2}$, 882 cm^{-1}), by molecular collision partners. In the present study Cl^* atoms are prepared in the presence of CH_4 or CD_4, under pseudo first-order conditions, by photolysis of ICl at 532 nm with a pulsed Nd:YAG laser. Quenching of Cl^* by CH_4 or CD_4 results in E-V excitation of the ν_4 asymmetric bending mode as observed by infrared (IR) fluorescence from the vibrationally excited products. Time-resolved IR fluorescence observations of $CH_4(\nu_4)$ and $CD_4(\nu_4)$ are consistent with a simple kinetic scheme involving direct E-V excitation of $CH_4(\nu_4)$ or $CD_4(\nu_4)$ followed by a slower collisional relaxation. The total quenching rate of Cl^* is reflected in the rise of the ν_4 fluorescence signal. The Cl^* total bimolecular quenching rate coefficients ($\pm 2\sigma$) obtained in this study at 298 $\pm$ 2 K are (1.9 $\pm$ 0.5) x 10^{-11} cm^3 $molecule^{-1}$ s^{-1} for quenching by CH_4 and (1.4 $\pm$ 0.9) x 10^{-10} cm^3 $molecule^{-1}$ s^{-1} for CD_4. Intensity measurements interpreted within this kinetic scheme indicate that the E-V channel for ν_4 mode excitation accounts for $\approx$30% of the total quenching of Cl^* by CH_4 and CD_4. It is remarkable that the E-V branching ratios are the same in both systems even though the $\nu_4 - Cl^*$ energy differences span a four-fold range from approximately ½kT (CD_4) to 2kT (CH_4).

TABLE OF CONTENTS

Page

Page

LIST OF FIGURES

LIST OF TABLES

ACKNOWLEDGMENTS

First and foremost, I wish to express my appreciation to my thesis advisor, Dr. David Dolson. His never-ending guidance, encouragement and understanding over great time and distance have made the completion of this endeavor a reality. Secondly, the support of my family has allowed me to devote the time necessary to attend classes, perform research, and compose this thesis. My wife Christie willingly took care of family responsibilities on many nights and weekends while I worked toward this goal. My daughters Stephanie and Kimberly, who never fully understood what daddy was working on, provided me more motivation than they will ever know.

INTRODUCTION AND PURPOSE

A. Importance of Cl + CH_4

The reaction between atomic chlorine and methane has been shown to play an important role in atmospheric chemistry. It is one of a few reactions that controls the amount of inorganic chlorine in the stratosphere (1), and it limits the loss of ozone via chlorine-radical catalytic cycles (2-5) while providing a sink for CH_4 molecules (6, 7). Several kinetic studies of this reaction have focused on the determination of rate constants for use in atmospheric and combustion models (8).

Historically, interest in the Cl + CH_4 reaction was heightened by a curious non-Arrhenius behavior of the low-temperature results in a laser flash-photolysis/resonance fluorescence study of reaction 1.1 by Ravishankara and Wine (9) over a temperature range from 221 – 375 K.

$$Cl(^2P) + CH_4 \rightarrow CH_3 + HCl \qquad \textbf{(1.1)}$$

Below 241 K, in reaction mixtures where He was used as the inert diluent gas, different rate coefficients were measured at both low and high CH_4 concentrations, and the resulting Arrhenius plot (Ln(rate coefficient) vs. inverse absolute temperature) shows substantial curvature in the lower temperature region. When a small amount of CCl_4 was

added, or the inert gas was changed from He to Ar, the expected linear relationship was observed. Thus, in summary, the bimolecular rate coefficient was found to be dependent upon the identity of the chemically inert gases in the reaction mixture. This non-Arrhenius behavior suggests that nonthermal reactant state distributions were the cause of the kinetic anomalies. The proposed model that Ravishankara and Wine presented to explain their results was centered on the hypothesis that the two spin-orbit states of chlorine have different reactivities towards methane. These two reactions can be illustrated as follows:

$$Cl^*(^2P_{1/2}) + CH_4 \xrightarrow{k_{1.2}} CH_3 + HCl \qquad \textbf{(1.2)}$$

$$Cl(^2P_{3/2}) + CH_4 \xrightarrow{k_{1.3}} CH_3 + HCl \qquad \textbf{(1.3)}$$

The first reaction shows the spin-orbit excited state of chlorine ($^2P_{1/2}$), while the second shows the ground state ($^2P_{3/2}$). Because reaction 1.3 is endothermic while reaction 1.2 is exothermic, it is believable that the ratio of bimolecular rate constants ($k_{1.2}/k_{1.3}$) might increase at lower temperatures. Additionally, the equilibrium population of the spin-orbit excited state would decrease. Thus, at low temperatures, it has been postulated that the spin-orbit excited state of chlorine reacts much faster than the ground state with methane. A spin-orbit excited Cl^* concentration greater than equilibrium (produced in flash photolysis laboratory experiments) with higher reactivity than the ground state Cl would lead to the positive deviation observed at low temperatures in the Arrhenius plot. Part of the answer to this assumption is to examine the importance of the electronic-to-

vibrational (E-V) energy transfer channel from electronically-excited chlorine atoms to the production of vibrationally-excited methane molecules (reaction 1.4).

$$Cl^*(^2P_{1/2}) + CH_4 \rightarrow Cl(^2P_{3/2}) + CH_4(\nu) \qquad \textbf{(1.4)}$$

Activity in this channel also removes Cl^* and adds to the total rate for Cl^* quenching by methane, but does so at the expense of the reactive channel. Specifically, we will examine the fraction of Cl^* + CH_4 collisions that quench the Cl^* state via the E-V process. This thesis reports experimental measurements of the branching fraction in the E-V transfer channel from the $Cl^*(^2P_{1/2})$ spin-orbit excited state of chlorine to the ν_4 vibrational level of CH_4 and CD_4 and the total absolute rate coefficients for the quenching of Cl^* by both methane isotopomers.

B. Nature of X^*

During the 1960s and early 1970s, several groups were investigating the importance of E-V transfer in the quenching of electronically-excited species (10-19). Many of these experiments have been reviewed by Lemont and Flynn (20). Following the completion of the experiments conducted for this thesis, Chichinin published an extensive review of the chemical properties of electronically excited halogen atoms (97). The nature of electronically-excited halogen atoms (X^*) will be explored here to provide a foundation for understanding the E-V quenching process.

All ground state halogen atoms can be described with the ground state electron configuration of ns^2np^5. The unpaired p-electron gives rise to two possible energy states, represented by the term symbols $^2P_{1/2}$ and $^2P_{3/2}$. From a quantum number perspective for a specific halogen atom, each of the valence p-electrons has the same principle quantum number (n = 2 for F, n = 3 for Cl …) and same electronic angular momentum (ℓ = 1) quantum number, as well as the same electron spin (s = 1/2). The total electronic angular momentum quantum number arising from the ground state electron configuration is L = 1, which defines a P term, and the total electron spin is S = 1/2, which leads to a spin multiplicity of M = 2S+1 = 2. Together, the values of L and S are conveyed in the term symbol, ^2P. A total electronic angular momentum, represented by quantum number J, arises from the coupling of the electron spin and the electronic angular momenta (either J = L+S = 3/2 or J = L-S = 1/2). Thus, two states are possible, represented by the term symbols $^2P_{1/2}$ and $^2P_{3/2}$. The 3/2 J state represents the ground state, and the 1/2 J state represents the spin-orbit excited state. This follows from Hund's rules, which require the higher J value to be the ground state in atoms with electron shells that are greater than half-full, as is the case with halogen atoms.

The spin-orbit properties of fluorine, chlorine, bromine, and iodine atoms have been summarized by Husain and Donovan (18) in Table 1.1. All transitions between ground states and spin-orbit excited states of atoms are forbidden by the electric dipole selection rules, or the Laporte rule, resulting in long radiative lifetimes of the $X^*(^2P_{1/2})$ states. Since spin-orbit coupling increases with atomic mass (the "heavy atom effect"), this leads to a larger ΔE which in turn leads to a greater radiative rate for the forbidden transitions.

For F and Cl, the $^2P_{1/2}$ - $^2P_{3/2}$ energy differences are comparable to lower-frequency vibrational separations in many molecules. For Br and I, however, the energy differences are large enough to allow the possible E-V excitation of high-frequency fundamentals (in the case of Br^*) and of more than one vibrational quantum in many small molecules (for Br^* and I^*). Magnetic dipole or quadrupole transitions are allowed between the $^2P_{1/2}$ and $^2P_{3/2}$ states, although they are much weaker than dipole transitions. Thus, for F and Cl where the spin-orbit coupling is modest and magnetic dipole and quadrupole transitions are extremely weak, the radiative lifetimes are quite long, and spontaneous emission has not been observed in experiments. On the other hand, the spin-orbit coupling is much larger for Br^* and I^*. This in turn enables transient concentrations of Br^* and I^* to be detected via time-resolved infrared fluorescence measurements, as will be discussed later.

Table 1.1: Spin-Orbit Properties in Halogen Atoms (18)

	$E\left(^2P_{1/2}-{}^2P_{3/2}\right)$		
Atom	cm^{-1}	kcal/mol	Radiative Lifetime (s)
F	404	1.15	830
Cl	882	2.52	83
Br	3685	10.53	1.1
I	7603	21.72	0.13

Houston (21) provides an excellent review of previous work on direct observations of E-V energy transfers from the spin-orbit excited states of both $Br^*(4^2P_{1/2})$ and $I^*(5^2P_{1/2})$. This process can be represented by the following:

$$X^*(^2P_{1/2}) + A(0) \rightarrow X(^2P_{3/2}) + A(\nu) \qquad \textbf{(1.5)}$$

In this scheme, the excited halogen atom $X^*(^2P_{1/2})$ transfers its energy to an acceptor molecule A. Molecule A is initially in a vibrational ground state A(0) and is excited to a higher vibrational level A(ν), and the halogen returns to its electronic ground state $X(^2P_{3/2})$.

Donovan, Husain, and Stephenson (22) were the first to observe E-V transfer from Br^*. Their flash photolysis experiment utilized ultraviolet absorption and allowed electronic transitions to monitor the bromine atomic states and HBr vibrational states during the transfer of energy from Br^* to HBr. Since this first flash photolysis study, reported in 1970, many different experimental methods have been applied in similar E-V studies. Several of these methods for the production of X^* and for measurements of the energy transfer kinetics will be discussed later.

C. Theories of Electronic-to-Vibrational (E-V) Energy Transfer

The transfer of energy from an electronically-excited halogen atom to the vibrations of a diatomic or polyatomic molecule has been reviewed by both Houston (21) and Yardley (23). Both of these provide not only a review of experimental techniques and results, but present fundamentally different theories for E-V transfer. Three of the leading theories to be discussed in this thesis are 1) resonance theories for long-range attractive forces, 2) curve-crossing mechanisms, and 3) quantum mechanical calculations.

1. Long-Range Attractive Forces

Short-range repulsive forces and long-range attractive forces are common to all atomic or molecular interactions and described by simple potential energy functions such as the Lennard-Jones potential. At long distances van der Waals forces attract any two species due to instantaneous dipoles in polarizable electron clouds surrounding atoms or molecules. This is true even for nonpolar interactions such as that between Cl^* and methane. Ewing (24) has reported that long-range interactions couple vibrational as well as electronic states so that the theories of Sharma and Brau (25) and Dillon and Stephenson (26-27), which were developed for vibrational-to-vibrational (V-V) energy transfer, can be extended to E-V transfer collisions with only minor changes.

First-order perturbation theory is used in this approach to calculate the probability of E-V transfer per molecular collision. Yardley (23) states the potential functions and probability equations, gleaned from the scientific literature, for electronic relaxation of an atom and simultaneous vibrational excitation of a molecular collision partner in three cases with transitions allowed by electric dipole or quadrupole moments. The case of Cl^* quenching by methane with excitation of the lowest energy bending vibration, ν_4, requires a (dipole-forbidden) $Cl^* \rightarrow Cl$ atomic relaxation via the electric quadrupole moment and an electric dipole allowed vibrational excitation. This quadrupole-dipole case was developed by Pritt and Coombe (28) and Donvan, Fotakis, and Golde (29) by extending Ewing's ideas. Applying the quadrupole-dipole potential and probability equations, stated by Yardley (23), to the Cl^* to $CH_4(\nu_4)$ E-V transfer process yields

equations 1.6 and 1.7, respectively, for the long-range potential function (30-32) and the E-V probability.

$$V(t) = (\tfrac{1}{2})Q^{Cl^*}\mu^{CH_4}[r(t)]^{-4} \qquad \textbf{(1.6)}$$

and

$$P_{if} = \left[\frac{\pi^2 \left|Q_{if}^{Cl^*}\right|^2 \left|\mu_{if}^{CH_4}\right|^2}{16\hbar^2 b^6 v^2}\right]\left[(1 + b\Delta\omega v^{-1})^2 e^{-2b\Delta\omega/v}\right] \qquad \textbf{(1.7)}$$

Long-range attractive forces theory accurately predicts the qualitative dependence of the quenching rate constant on ΔE and Δv, however; the original theoretical foundation considered resonant or near resonant energy transfer, and so this result may not be applicable for E-V transfer at very large ΔE.

2. Curve-Crossing Mechanisms

Another E-V transfer theory was introduced by Nikitin (33-35) and is based on the idea that E-V transfer involves crossing between the zero-order potential energy curves (or surfaces) corresponding to X^* + M(0) and X + M(v). The theory was expanded by Bauer, Fisher, and Gillmore (36). Hypothetical potential energy curves are shown qualitatively

for the X^* + M(0) and X + M(ν) systems in Figure 1.1. The X^* and M(ν) energies chosen for the figure correspond to Cl^* and $CD_4(\nu_4)$. The approaching species move along the lower curve until they reach the circled intersection region, wherein the reactants undergo a nonadiabatic transition and begin following the upper curve as the collision partners separate. This transition corresponds to the electronic relaxation of the halogen atom and the vibrational excitation of the molecular collision partner. A successful quenching collision requires that a curve-crossing event occur only once during the collision. There are two possible pathways to achieve this quenching, as shown in Figures 1.2 and 1.3. These two figures illustrate possible collision trajectories in the circled intersection region from Figure 1.1. If there is no curve crossing or if the curve crossing occurs twice during the collision, then the outbound trajectory remains on the X^* + M(0) curve and quenching does not occur.

This nonadiabatic transition can be described by the Landau-Zener formula for the probability of crossing (33-35, 37-41). For a single crossing the probability of a transition from the X^* + M(0) zero-order curve to the X + M(ν) curve is given by

$$P_{EV} = 1 - e^{\left(\frac{-2\pi |V_{if}|^2}{\Delta F \hbar \nu}\right)} \qquad \textbf{(1.8)}$$

Where V_{if} is the matrix element for the potential interaction, and ΔF is a measure of how fast the two surfaces approach each other. A common estimate is $\Delta F \approx \Delta E\alpha$, where ΔE is the M(ν)-$X^*$ energy difference and α^{-1} is the length over which the coupling between

zero-order potential curves is strong. Equation 1.8 provides a means to predict qualitatively the features of E-V transfer. For example, the matrix element, V_{if}, includes the vibrational contribution, which decreases rapidly as Δv increases. Also, when ΔE is not too large, P_{EV} falls exponentially as ΔE increases. This latter behavior is followed later in Figure 1.4, where the exponential dependence (linear behavior in the semilog plot) is better for $\Delta E \leq 100$ cm^{-1}.

3. Quantum Mechanical Calculations

Houston, in his earlier review (21), summarized quantum mechanical calculations by Zimmerman and George (42-44), who performed calculations for the first four halogens and H_2, HD and D_2. Houston's review focused only upon the Br^* and I^* calculations. The calculations ignored the effects of rotation and long-range attraction and focused only on collinear configurations. Predicted Br^* E-V probabilities followed the order HD > H_2 > D_2, in agreement with experimental results (45). Further, the main quenching contribution from all three species was predicted to be from collisions that leave the hydrogen in its first vibrationally excited level. The results for I^* also were in good agreement with experiment. Again, HD was predicted to have the largest quenching cross-section, followed by H_2 and D_2. It was also correctly predicted that the quenching would be slower than that of Br^*. Also in reference (43) it was predicted that the Cl^* quenching probabilities would follow the (experimentally confirmed) order H_2 > D_2. Here Cl^* quenching must follow an E-R,T pathway(s) as the vibrational levels are

inaccessible to the Cl^* energy. Due to the serious challenges of performing accurate theoretical calculations involving the spin-orbit halogen states, theory lags experimental results in this area. More recent theoretical treatments are referenced in the 2006 review by Chichinin (87).

Figure 1.1: Potential Energy Curves for X^* + M(0) and X + M(ν)

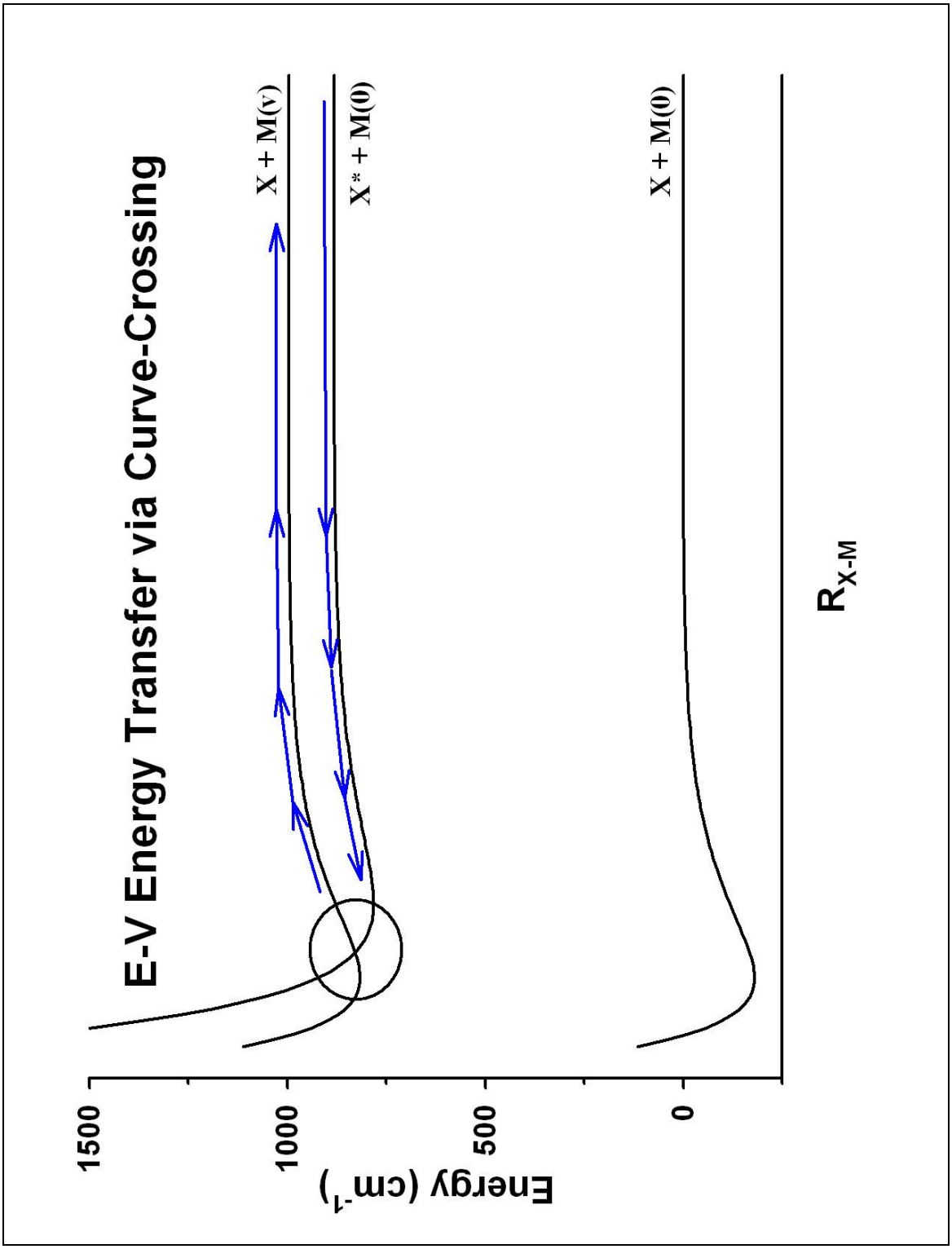

Figure 1.2: Expanded Curve Crossing Region (Quenching Pathway #1)

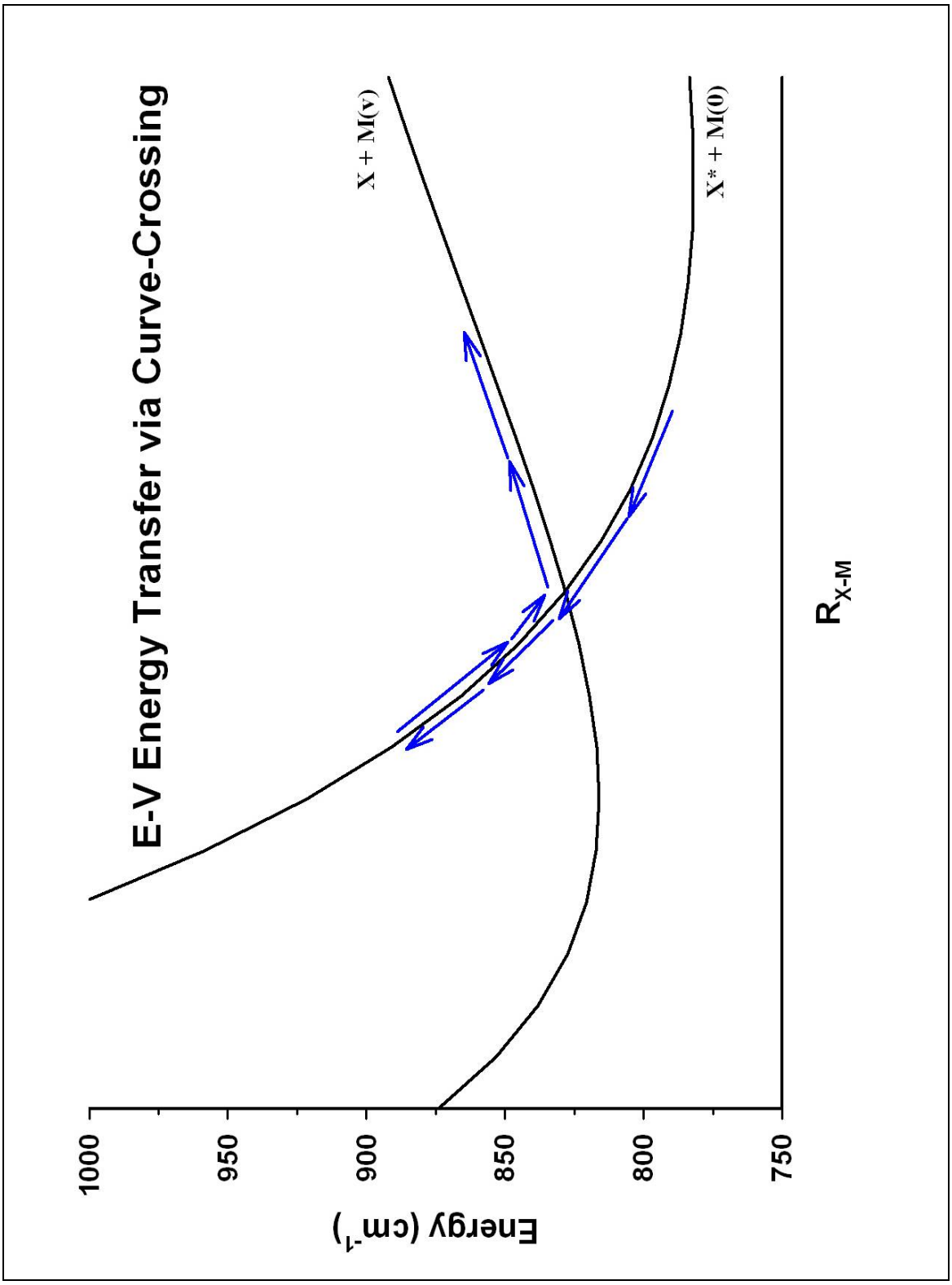

Figure 1.3: Expanded Curve Crossing Region (Quenching Pathway #2)

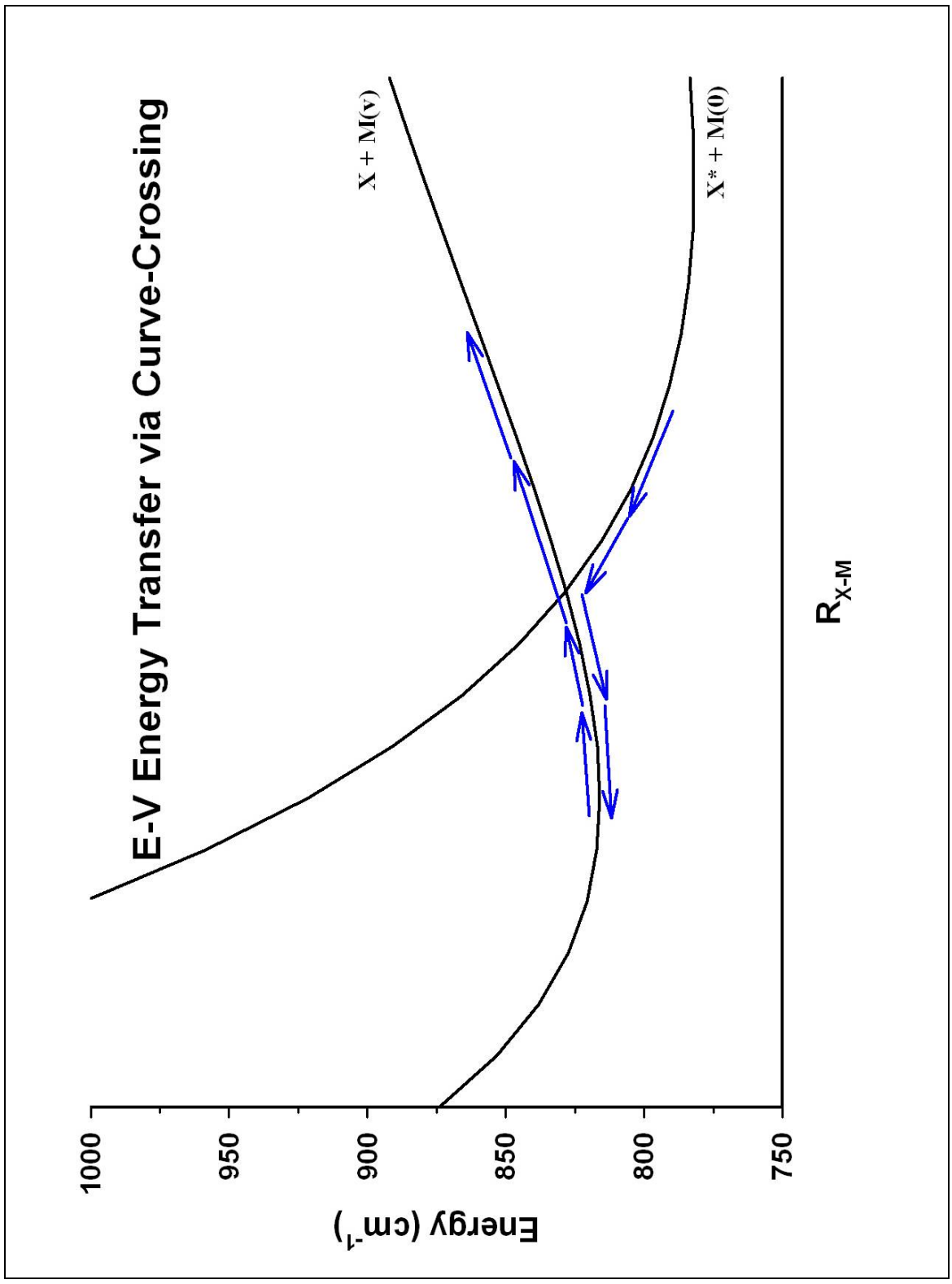

D. Experimental Methods of Cl^* Quenching

The collisional deactivation of spin-orbit excited chlorine atoms $Cl^*(^2P_{1/2})$ has been the focus of much attention over the past three decades. Several methods with varying quantum yields have been described for the production of Cl^*, each of which is rooted in the photolysis of a Cl-containing precursor through the use of a laser or a flash lamp. Detection of Cl^* has also been accomplished by various methods, including laser magnetic resonance (LMR), diode laser absorption spectroscopy, and resonance enhanced multiphoton ionization (REMPI). A brief description of both Cl^* production and detection will follow, as well as a review of experimental results.

Park, Lee, and Flynn (46) have provided quantum yield data for the production of Cl^* from photolysis of the following precursors: Cl_2, HCl, ICl, NOCl, $SCCl_2$, PCl_3 and CCl_4. The photolysis laser was a UV pulsed excimer which has been described previously (47, 48). Each of the Cl precursors is excited and proceeds to dissociate on a short time scale. Quantum yield (φ^*) for Cl^* production is defined as the following

$$\varphi^* = \frac{N(^2P_{1/2})}{N(^2P_{1/2}) + N(^2P_{3/2})} \qquad \textbf{(1.9)}$$

where N is the number of Cl atoms in their respective states. The determination of φ^* is based on a diode laser gain versus absorption technique based upon the forbidden

$Cl^*(^2P_{1/2}) \leftrightarrow Cl\ (^2P_{3/2})$ transition, and is explained in detail elsewhere (49-51). Table 1.2 summarizes the quantum yield results.

Table 1.2: Relative Yields (φ^*) for Producing $Cl(^2P_{1/2})$ Atoms (46)

Cl Precursors	Photolysis Wavelength (nm)	$\varphi^* = \frac{[Cl^*]}{([Cl^*]+[Cl])}$
S_2Cl_2	193	0.20 ± 0.03
S_2Cl_2	248	0.21 ± 0.03
S_2Cl_2	308	0.48 ± 0.06
PCl_3	193	0.33 ± 0.03
PCl_3	248	0.44 ± 0.03
CCl_4	193	0.15 ± 0.03
Cl_2	308	≤ 0.01
Cl_2	340-355	≤ 0.01
$SCCl_2$	248	0.33 ± 0.03
HCl	193	0.18 ± 0.03

A similar study to determine quantum yields of Cl^* via photolysis was undertaken by Tiemann, Kanamori, and Hirota (52). An excimer laser (193 nm ArF or 248 nm KrF) was also used to produce Cl^* atoms from precursor molecules. Table 1.3 summarizes their results. Absolute rate coefficients obtained from the pressure dependence of the Cl^* quenching rates by the photolytic precursor molecules also are presented.

Table 1.3: Relative Yields and Collisional Quenching Rates at 295K of $Cl(^2P_{1/2})$ Generated by Photodissociation (52)

Cl Precursor	Relative Yield	Quenching Rate Coefficient (cm^3 $molecule^{-1}$ s^{-1})	Wavelength (nm)
HCl	0.33 ± 0.03	$(1.2 \pm 0.2) \times 10^{-11}$	193
CH_3Cl	0.33 ± 0.03	$(5 \pm 2) \times 10^{-11}$	193
CH_2Cl_2	0.33 ± 0.03	$(2 \pm 1) \times 10^{-10}$	193
C_6H_5Cl	0.16 ± 0.02	$(5 \pm 1) \times 10^{-10}$	193
PCl_3	0.37 ± 0.02	$(1.3 \pm 0.2) \times 10^{-11}$	193
PCl_3	0.44 ± 0.02	$(1.3 \pm 0.2) \times 10^{-11}$	248

The two previous methods for Cl^* production have involved the use of excimer lasers operating in the ultraviolet (UV) region of the spectrum. Mashnin, Chernyshev, and Krasnoperov (53) utilized a pulsed dye laser pumped by a XeCl excimer laser as the source of photolyzing radiation within the wavelength range of 437 to 532 nm, which is within the visible spectrum. The iodine monochloride (ICl) precursor was irradiated at several different wavelengths within this range, and the results are recorded in Table 1.4.

LMR techniques have previously been employed for the detection of Cl^* (54-56). In this technique, the gases in the photolysis cell are inserted into the cavity of a CO_2 laser and subject to oscillating and constant magnetic fields. The CO_2 laser is tuned to the appropriate ΔE for the transition being observed, which for Cl^* to Cl is 882 cm^{-1}. The photolyzing laser and the CO_2 laser beams cross at a shallow angle in the reaction cell to ensure a large overlap of the beams. Exiting CO_2 laser radiation then proceeds to a cooled photoresistor, and the signal is detected by a lock-in amplifier, digitized, and then transferred to a computer for processing. The resulting kinetic curves are the time-resolved signals of either the absorption or gain of the CO_2 laser radiation.

Diode lasers have also been employed to observe the transition from Cl^* to Cl. Diode lasers are useful to probe Cl since Doppler profile measurements provide the precise translational energy distributions for the photodissociated Cl atoms, as well as relative yields of excited Cl ($^2P_{1/2}$) and ground state Cl ($^2P_{3/2}$) atoms (46). From the work of Davies and Russell (57), the resolution of diode spectroscopy is high enough to monitor Cl on a single hyperfine component, typically the strongest transition from $^2P_{3/2}$ (F = 3)

$\rightarrow {}^2P_{1/2}$ (F = 2). Following excitation of the Cl atoms, the resulting absorption or gain in the diode laser energy is recorded on a photoconductive detector, amplified, digitized, and signal averaged.

Another technique used to detect Cl and Cl^* is REMPI via the pumping of two-photon-allowed transitions in the wavelength region of 230 – 245 nm (58). Chlorine atom detection was accomplished by two-photon resonant, three-photon ionization using UV light. A dye laser pulsed with a 150 mJ excimer pulse was used to cover the above wavelength region.

Table 1.4: Yield of $Cl^*({}^2P_{1/2})$ Atoms in the Photodissociation of ICl (53)

Wavelength (nm)	Cl^* Quantum Yield
437	0.41 ± 0.02
450	0.58 ± 0.02
455	0.66 ± 0.02
460	0.73 ± 0.02
465	0.75 ± 0.02
470	0.76 ± 0.03
475	0.78 ± 0.02
480	0.79 ± 0.03
485	0.77 ± 0.02
490	0.76 ± 0.03
495	0.77 ± 0.02
500	0.76 ± 0.02
505	0.75 ± 0.02
510	0.73 ± 0.03
520	0.71 ± 0.03
532	0.58 ± 0.03
266	0.65 ± 0.06

Until recently, few attempts have been made to investigate what role a reagent's initial spin-orbit state plays in the determination of reaction rates and the distribution of energy

into products. The majority of past experiments that studied initial energy selection have been limited to translational (59) and vibrational (60-62) degrees of freedom. In theory, the specificity of a reagent's spin-orbit state involves the nonadiabatic transition of multiple potential energy surfaces (PES) (63).

The study of the reaction between atomic chlorine and hydrogen to produce hydrogen chloride and atomic hydrogen has been explored to provide insight into spin-orbit reactivity. This reaction is the simplest chlorine atom reaction.

$$Cl(^2P) + H_2 \rightarrow HCl + H \qquad \textbf{(1.10)}$$

Lee, Lai, Liu, and Chang (64) studied reaction 1.10 to understand the spin-orbit state-specificities by altering the initial state distribution and then measuring dynamical observables (primarily the rotational state distribution of the HCl product molecules) to see how they vary with the initial distributions. Previous to this work, the general agreement between experiment and theory led to a conclusion that this reaction is adiabatic, meaning the spin-orbit excited Cl^* state is nonreactive to H_2 (65). Two Cl source beams were used. The photolysis of Cl_2 at 355 nm was used for the ground-state Cl atom beam due to the low yield of Cl^* at this wavelength (less than 1.6%). A discharge approach (3-5% Cl_2 seeded in He at 15 atm, discharged at 1.1kV dc) was adapted to generate the chlorine beam with both ground and spin-orbit excited states. Through the study and comparison of the excitation function results for both the photolysis and discharge Cl beams over a range of collision energies, it was revealed that

for either the para-hydrogen (p-H_2) or normal-hydrogen (n-H_2) target, the rise of the cross sections in the post-threshold region is steeper for the discharged Cl beam than for the photolyzed Cl beam. The magnitude of the ratio between the reaction cross sections of n-H_2 to p-H_2 at a given collisional energy is noticeably different, signifying non-negligible reactivity of the spin-orbit excited chlorine atoms from the discharged source.

Further work by Lee and Liu (66) continued the exploration of spin-orbit excitation in the chlorine/hydrogen reaction. This study employed the two Cl source beams described above and found that the excited Cl^* atom is more reactive to H_2 than the ground-state atom by approximately a factor of six. Dong, Lee, and Liu (67) confirmed and quantified the nonadiabatic reactivity of Cl^* with H_2 in a recent publication.

In direct contrast to the above work of Liu, *et al*., Alexander, Capecchi, and Werner (68) predict that the ground-state Cl will be much more reactive than the spin-orbit state. This group used *ab initio* potential energy surfaces and exact quantum scattering calculations to explore the extent of electronic nonadiabaticity in the Cl + H_2 reaction. It was observed that the cross section for the Cl^* (nonadiabatic) reaction is small in comparison with that for reaction of the ground state (adiabatic). Only at very low collisional energies (<5 kcal/mol) does the Cl^* pathway begin to dominate, due to the greater internal energy which does allow the reaction energy barrier to be overcome. This theoretical treatment is in direct disagreement with the work of Liu and coworkers experimental work.

Alexander, *et al.* followed their theoretical work by reporting a combined experimental and theoretical determination of the differential cross sections of reaction 1.10 at three collisional energies (3.85, 4.25, and 5.85 kcal/mol) (69). The result of this work suggests that the potential energy surfaces may underestimate the degree of rotational excitation of the HCl products and that the excited Cl^* spin-orbit state plays a minor role in the reaction.

Due to this disagreement relating to the role of spin-orbit excited Cl^* atoms in the reaction with H_2, it is clear that more investigation in both theoretical and experimental studies is needed. This is currently one of the major unresolved problems in the dynamics of elementary chemical reactions. Unfortunately, until this disagreement is settled, it is unlikely that any further theoretical studies will be performed on more complicated systems, including the reactions of Cl and Cl^* with CH_4.

E. What is Known about $Cl^* + CH_4/CD_4$

Many previous studies have investigated the kinetics of the reaction between Cl and CH_4 (9, 70-75). However, the reactions between Cl and deuteriomethane isotopomers (other than CH_4) have received little attention. As stated earlier, the reaction of Cl with CH_4 is one of the most important reactions that control the distribution of inorganic chlorine in the atmosphere. Similarly, since 99% of the partially deuterated methane in the atmosphere is CH_3D, the reaction rate constant of CH_3D should control the vast majority of the D content in atmospheric methane in terms of methane destruction with Cl (76). Prior to 1997, the only indirect method used to determine a rate constant ratio between

CH_4 and CD_4 was to irradiate a mixture of Cl_2 and CH_4/CD_4 with ultraviolet light in a static cell over a temperature range of 300-475 K (70). The ratio of the rate constants was determined through the mass-spectrometric analysis of the isotopic comparison of the products.

Matsumi, *et al*. (76) undertook a study to determine the absolute rate constants for the reaction of Cl and Cl^* atoms with deuterated methanes at room temperature. Their experiment utilized vacuum-ultraviolet (VUV) laser-induced fluorescence to monitor both Cl and Cl^* spin-orbit states and derive separate rate coefficients for their removal in collisions with the reaction partners. This technique allowed for the direct observations of the different reactivities of the Cl and Cl^* states in collisions with the deuterated methanes. The total quenching rate coefficients for the removal of Cl^* by all physical and reactive channels determined in this investigation are presented below in Table 1.5:

Table 1.5: Reaction Rate Coefficients for Cl/Cl* + Reactant Molecules (76)

Cl Atom	Molecule	Rate Coefficient (cm^3 $molecule^{-1}$ s^{-1})
Cl ($^2P_{3/2}$)	CH_4	$(10.0 \pm 1.0) \times 10^{-14}$
Cl ($^2P_{3/2}$)	CH_2D_2	$(7.0 \pm 0.8) \times 10^{-14}$
Cl ($^2P_{3/2}$)	CD_4	(0.82 ± 0.10) x 10-^{14}
Cl^* ($^2P_{1/2}$)	CH_4	$(3.0 \pm 0.3) \times 10^{-11}$
Cl^* ($^2P_{1/2}$)	CH_2D_2	$(11 \pm 1) \times 10^{-11}$
Cl^* ($^2P_{1/2}$)	CO_2	$(1.2 \pm 0.1) \times 10^{-11}$

The first direct comparison of Cl and Cl^* reactivity with CH_4 was accomplished by Zare, *et al*. (85). The ground state Cl ($^2P_{3/2}$) atom reaction with methane is endothermic by 600 cm^{-1} (86), whereas the spin-orbit excited Cl^* ($^2P_{1/2}$) atom reaction is exothermic by 281

cm^{-1} as a result of the 882 cm^{-1} difference in the spin-orbit energy of Cl^* compared to Cl. (86). Although the Cl^* reaction is exothermic, it is possible that the reaction barrier might be higher than that of the ground-state Cl due to nonadiabatic interaction near the barrier. The group tested this possibility by tuning the collision energy through a range of 0.13-0.16 eV. The result obtained was that the $Cl^* + CH_4$ reaction was not important in this energy range. Instead, they suggest the dominant reaction occurs between ground-state Cl atoms with vibrationally-excited CH_4 molecules ($\nu = 2$ or 4). Therefore, this study concludes that the non-Arrhenius behavior of this reaction at low temperatures cannot be explained by Cl^* reactivity.

Because the E-V quenching of Cl^* by methane produces vibrationally excited methane and ground state Cl atoms, it is prudent to consider whether or not there is an increase in the Cl atom reactivity with vibrationally excited methane. In fact, the $Cl + CH_4$ reaction has also been investigated by vibrationally exciting the methane molecule. Simpson, et al. (77, 78) measured the relative state-dependent reaction cross-sections and product angular and internal state distributions for this reaction. Through the direct pumping of the asymmetric CH stretch (ν_3) of CH_4 with an IR laser, it was demonstrated that the excitation of one quantum of the stretch enhances the reaction probability by a factor of approximately 30 and produces more forward- and side-scattered HCl product with more rotational energy than observed for the ground-state reaction. Following these studies, Kandel and Zare (79) expanded the investigations of the ground-state reaction to a wider range of collision energies. Instead of measuring the HCl product, they probed the CH_3 produced by the reaction. The result was the observation of products with more

translational energy than could be accounted for by the energetics of the reaction. This observation was explained by hypothesizing the participation of reactions involving thermally populated excited states of the low-frequency bending modes of CH_4, suggesting that excitation of the umbrella (ν_4) and/or torsional (ν_2) modes of CH_4 also enhance methane reactivity with Cl atoms. The enhancement was estimated to be 200 times larger than the Cl + CH_4 (v = 0) reaction. Work accomplished in the late 1970s by Hsu and Manuccia indicated that pumping the CH_2 rocking mode (ν_7) of CH_2D_2 enhances the reaction rate with Cl (80-82). Vijin, *et al*. (83) contrast this observation by noting no appreciable enhancement in reactivity when directly pumping the ν_4 mode of CD_4 in a mixture of CH_4/CD_4 and measuring the isotopic fractionation of products. This result was also experienced by Chesnokov, *et al*. (84) who pumped the asymmetric stretch of CH_4 and did not observe any reaction enhancement.

Chichinin (56) has previously investigated Cl^* quenching rate coefficients for twenty different molecules. This study suggests that the E-V energy exchange is apparently the dominate route for Cl^* quenching in most cases. As noted earlier, the two main theories of energy transfer are long-range attractive forces and curve crossing. Each of these theories predicts that the rate constant for deactivation of Cl^* by a quencher M may be expresses as follows:

$$k_{qM} = \sum A(I_i / \nu_i) e^{\left(\frac{-|\Delta E_i|}{B}\right)} \qquad \textbf{(1.11)}$$

which is the summation over the vibrational modes of the quencher, I_i and ν_i are the intensity and the frequency of the *i*th absorption band of the quencher, $\Delta E = h\nu - E_{Cl^*}$ is the energy defect of the E-V transfer process, and A and B are parameters determined to be 145 and 77 cm^{-1}, respectively. Table 1.6 lists the cases for which the E-V energy exchange seems to be the dominate pathway. A plot of the logarithm of the experimental rates against the energy defect (ΔE) is shown in Figure 1.2. The data, with few exceptions, all fall near to the same line, which suggests that these systems are dominated by a similar E-V mechanism. Specifically for CH_4 and CD_4, the lower ΔE value for the CD_4 is in keeping with its larger quenching rate coefficient. However, whether or not it also leads to a more probable E-V channel remains to be determined in this thesis.

The second part of this thesis will cover the experimental equipment, chemicals, and procedures used to acquire the data presented here. The experimental results will be presented in the third part, along with a discussion of the data.

Table 1.6: E-V Transfer Data from Cl* to Molecule M (56)

Molecule	k (Rate Coefficient cm^3 $molecule^{-1}$ s^{-1})	Ln k	Vibrational Frequency (cm-1)	ΔE (cm-1)	|ΔE|
ICl	3.3×10^{-13}	-26.245	381	501	501
O_3	7.0×10^{-12}	-25.685	1042	-160	160
CO_2	9.0×10^{-12}	-25.434	667	215	215
NOCl	1.8×10^{-11}	-24.741	596	286	286
N_2O	6.3×10^{-12}	-25.791	1285	-403	403
NF_3	2.2×10^{-10}	-22.237	906	-24	24
SO_2	1.8×10^{-11}	-24.741	1361	-479	479
$COCl_2$	3.0×10^{-10}	-21.927	850	32	32
PCl_3	1.3×10^{-11}	-25.066	504	378	378
CH_4	1.9×10^{-11}	-24.687	1306	-424	424
CD_4	1.3×10^{-10}	-22.764	996	-114	114
CCl_4	1.8×10^{-10}	-22.438	776	106	106
CF_4	2.7×10^{-11}	-24.335	1283	-401	401
CCl_3F	2.2×10^{-10}	-22.237	847	35	35
CF_3I	1.0×10^{-10}	-23.026	1151	-269	269
CH_3Cl	5.0×10^{-11}	-23.719	732	150	150
CH_2Cl_2	2.0×10^{-10}	-22.333	758	124	124
CF_2Cl_2	1.8×10^{-10}	-22.438	1001	-119	119
SiF_6	1.4×10^{-10}	-22.689	1031	-149	149
SF6	1.8×10^{-10}	-22.438	947	-65	65

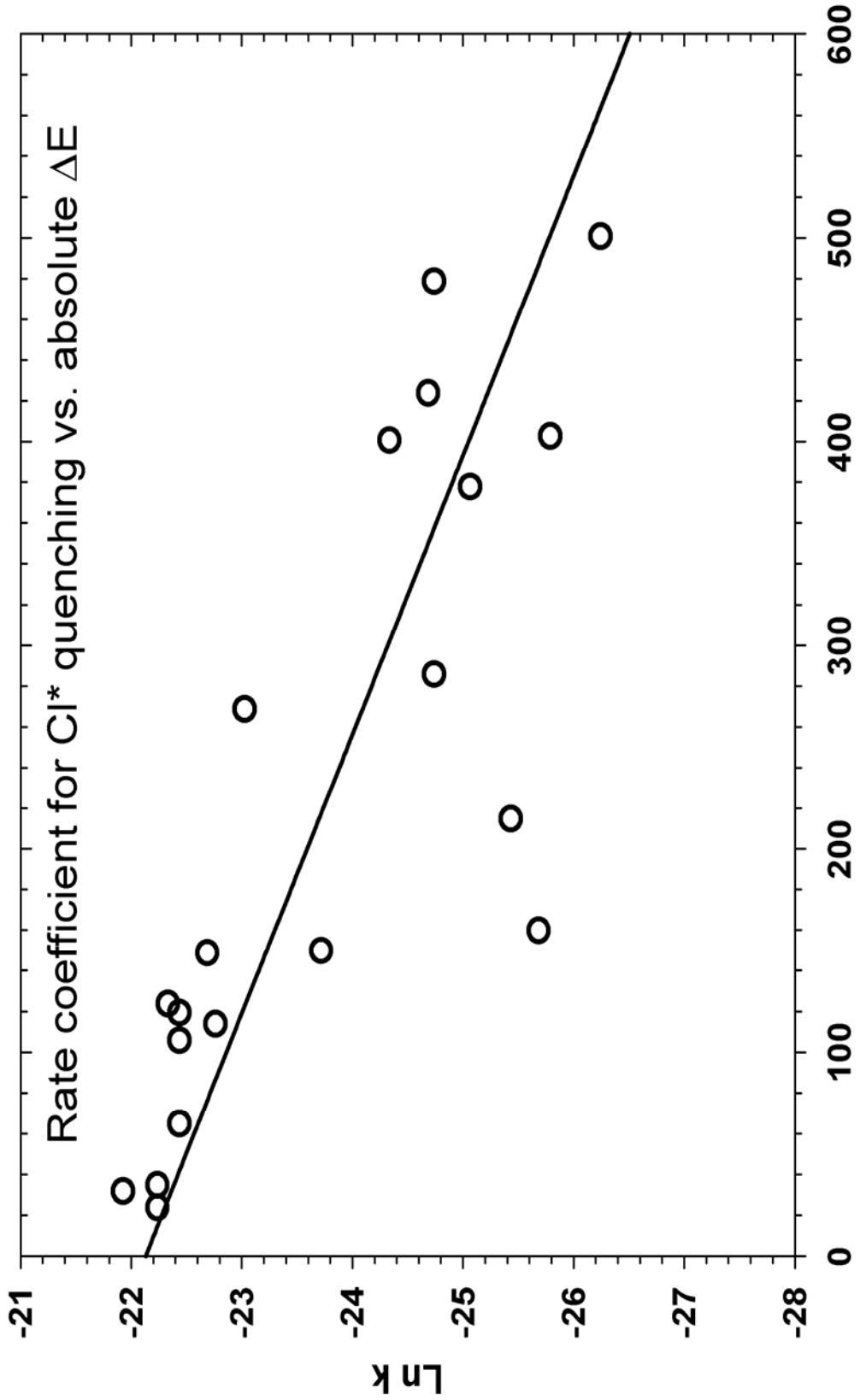

Figure 1.4: Ln (Rate Coefficient) vs. ΔE

EXPERIMENTAL

All the experiments in this thesis were conducted to monitor the reaction below:

$$Cl^* + CH_4 / CD_4 \rightarrow Cl + CH_4 / CD_4(v) \qquad \textbf{(2.1)}$$

In each experiment, the concentrations of either CH_4 or CD_4 were much greater than that of the initial concentration of Cl^* to allow for pseudo first-order kinetics. The initial ICl concentration was fixed, as was the laser pulse energy which resulted in a constant Cl^* concentration throughout the experiments. Only the CH_4 or CD_4 concentrations were varied and the observations were fit to exponential rise and decay curves.

A. Equipment and Setup

1. Laser

The laser used in the experiments described in this thesis was a Spectra Physics DCR-11 pulsed Nd:YAG at 60 mJ/pulse at 10 Hz. This laser uses triply ionized neodymium (Nd^{3+}) from a neodymium-doped yttrium aluminum garnet (YAG) rod as an active medium. The lasing transition produced photons at a fundamental wavelength of 1064 nm. A pulse width of 8 ns was obtained via timing and polarization of the laser beam using an electro-optic Q-switch comprised of a polarizer, a quarter-wave plate, and a

Pockels cell. The fundamental 1064 nm beam can be converted into various harmonics through the use of non-linear crystals of potassium dideuterium phosphate (KD^*P). The second harmonic at 532 nm was obtained by passing the fundamental through a single crystal. Both the fundamental and harmonic beams are collinear when they leave the laser. The separation of these beams was accomplished using a fused-silica Pellin-Broca prism within an optics chamber on the optics table. The fundamental beam was captured in a beam dump, and only the second harmonic was deflected with a fused silica right angle prism to the photolysis cell for use in the experiments.

The 532 nm second harmonic beam was used to produce spin-orbit excited chlorine atoms (Cl^*) from an iodine chloride (ICl) precursor via reaction 2.2.

$$ICl + h\nu(\lambda = 532nm) \rightarrow I + Cl^* \qquad \textbf{(2.2)}$$

This reaction has been reported to produce Cl^* atoms with a quantum yield of 58 ± 3 % (53). The 8 ns laser pulse effectively prepares Cl^* atoms "instantaneously" on the time scale of the subsequent kinetic events. Thus, the timing of the laser pulse is the time zero point for the kinetic observations. A simple, electrically isolated, battery-powered photodiode circuit is used to detect the laser firing and to provide a trigger signal for the digital oscilloscope to record the detector response upon each laser shot.

It is important to consider the reaction energetics at this point. Since both momentum and energy must be conserved, the energy distribution following the reaction must equal

the energy available at the initiation of the reaction. Equation 2.3 shows the energy change for reaction 2.2

$$\Delta E = E_P - (D_{(ICl)} + E_{CL^*}) \quad \textbf{(2.3)}$$

where E_p is the energy of the incident photon, $D_{(ICl)}$ is the dissociation energy of ICl, and E_{Cl^*} is the energy of the spin-orbit excited chlorine atom product. Performing the necessary calculations results in the following values: $E_p = 3.73 \times 10^{-19}$ J, $D_{(ICl)} = 3.45 \times 10^{-20}$ J, and $E_{Cl^*} = 1.75 \times 10^{-20}$ J. Inserting these values into equation 2.3 shows $\Delta E = 1.12 \times 10^{-20}$ J. This resulting "excess" energy is partitioned between the product atoms as translational energy, and could give rise to translational-to-vibrational (T-V) energy transfer to the molecules under study. Given the conservation of momentum, equation 2.4 can be written

$$(M_I \times V_I) = (M_{Cl^*} \times V_{Cl^*}) \quad \textbf{(2.4)}$$

where M is the mass and V is the velocity of the respective atoms. To determine the translational energy of the Cl^* atom, this equation can be rewritten as:

$$E_{Cl^*,trans} = \left(\frac{M_I}{M_I + M_{Cl^*}} \right) (\Delta E) \quad \textbf{(2.5)}$$

Inserting the appropriate values above results in $E_{Cl^*,trans} = 8.7 \times 10^{-21}$ J, which converts to 442 cm^{-1}. The average translational energy is given by

$$\langle E_{trans} \rangle = 3/2(kT) \quad \textbf{(2.6)}$$

where (kT) is approximately 208 cm^{-1}, resulting in an average translational energy of 312 cm^{-1}. Therefore, it is shown that the translational energy of the Cl^* atom resulting from reaction 2.2 is only 1.4 times the average. In order to remove this excess translational energy from the reaction system, argon gas is introduced to the reaction mixture.

A comparison of the collision numbers between Cl^* and Ar to that of Cl^* with CH_4 is necessary to ensure that Cl^* is thermally equilibrated when reacting with CH_4. In the experiments conducted for this research, typical CH_4 pressures varied between 0.1 and 0.6 torr, and an Ar pressure of 5 torr was constant. Taking a typical CH_4 pressure of 0.4 torr, the collision rate is approximately 6.2×10^5 s^{-1} $torr^{-1}$, which translates to 4 μs per quenching collision. Similarly, for Ar at 5 torr, the collision rate is approximately 1×10^7 s^{-1} $torr^{-1}$, which translates to 0.02 μs per quenching collision. Thus dividing 4 μs by 0.02 μs results in 200 collisions with Ar per each collision with CH_4. Therefore, it is reasonable to presume any initial translational energy possessed by the Cl^* atom at the completion of reaction 2.2 is successfully removed by the addition of Ar gas to the reaction mixture.

The second harmonic beam exiting the laser had a characteristic cross-sectional intensity profile of a "doughnut" shape due to the unstable resonator design of the laser cavity. The Beer-Lambert law (equation 2.7) was used to determine the fraction of photons transmitted by the ICl.

$$I = I_0 e^{-\sigma N \ell} \tag{2.7}$$

In this equation, σ is the absorption cross section in cm^2, N is the number density of photolytic precursor molecules in molecules/cm^3, and ℓ is the laser path length in centimeters through the cell. Equation 2.7 can be rewritten to give the fraction of photons absorbed by these gases

$$f = (1 - \frac{I}{I_0}) = (1 - e^{-\sigma N \ell}) \approx \sigma N \ell \tag{2.8}$$

where the approximation is only valid for $\sigma N \ell << 1$. The number of photons produced per laser pulse is given by

$$n = \frac{E\lambda}{hc} = 5.0 \times 10^{12} (E\lambda) \tag{2.9}$$

where E is the laser energy in mJ and λ is the laser wavelength in nm. The diameter of the laser beam was 6.4 mm at the laser output and diverged to ~ 11 mm at the photolysis

cell. This resulted in a cross-sectional area, a_b, of about ~ 1 cm^2. The fraction of excited Cl^* atoms generated photolytically may then be calculated by

$$fraction\ excited = \frac{[Cl^*]_0}{[N]} = \frac{5.03 \times 10^{12} (E\lambda)(\sigma)(\varphi_{Cl^*})}{a_b} \quad \textbf{(2.10)}$$

where φ_{Cl*} is the quantum yield for generating the spin-orbit excited species Cl^* from its precursor at wavelength λ. For ICl, $\varphi = 0.58$ and $\sigma = 1.08 \times 10^{-19}$ cm^2 at $\lambda = 532$ nm, and E = 60 mJ, resulting in photodissociation of approximately 1% of the ICl precursor to produce Cl^*(53). This shows that the conditions are kept within bounds to allow for pseudo first-order kinetics.

2. Photolysis Cell

The photolysis cell used in this experiment is shown graphically in Figure 2.1. The reactant gases were introduced into the photolysis cell via calibrated flow controllers, which will be described later in this section. After calibration, the flow controllers were set to calculated target values and the glass outlet stopcock to the vacuum pump was adjusted to obtain the desired pressure within the cell.

The viewing salt window (KCl or NaCl) was situated at a 90-degree angle from the incident laser beam. A narrow spectral band pass filter was placed between the salt window and the detector to transmit the vibrational emission band of interest. Quartz windows were used to allow laser beam transmission through the cell. All of the

windows were sealed to the cell using either Apiezon black wax or with a Viton o-ring. The incident laser beam was captured behind the photolysis cell using a beam dump. The cell system was also connected to a conventional vacuum line using Pyrex tubing with Cajon o-ring compression fittings. The use of metal was minimized and consisted of stainless steel and inconel.

An access port, located near the photolysis region of the cell, was connected to two MKS capacitance manometers of 10 and 100 torr full scale ranges. These manometers were used to measure the total pressure of the gas mixtures under study. The manometers were zeroed while the cell was open to the diffusion pump on the vacuum line.

3. Gas Handling

A typical gas handling system was used to direct the gases to the photolysis cell or to volumes for storage or mixing. The gas rack had a Pyrex manifold and storage volumes, two capacitance manometers of 10 Torr and 1000 Torr full scale ranges, ports for the addition of smaller volumes, a roughing vacuum pump, and a high vacuum system (ion gauge, liquid nitrogen trap, and an oil diffusion pump using Dow DC-704 silicone oil) capable of $<10^{-5}$ torr. Connecting tubing was mostly Pyrex with 316 stainless steel. Copper lines were used to connect to the non-corrosive cylinder gases. Whitey brass and stainless steel valves of various designs were used where elevated pressures were expected. The stainless steel valves were used for corrosive gases exposure. Connections were made using Swagelok fittings or Cajon o-ring compression fittings.

The glassware was interconnected with vacuum o-ring joints (Ace), o-ring compression fittings (Cajon), and glass stopcocks (Ace). All o-rings were Viton, lubricated with DuPont Krytox fluorinated vacuum grease.

The MKS flow controllers were re-calibrated prior to each experiment by measuring the rate-of-rise of the gas pressure in a fixed volume using a 10, 100, or 1000 torr full scale MKS capacitance manometer and a manual stopwatch. This was accomplished by setting an appropriate flow on the flow controller, closing the outlet stopcock to the vacuum pump, then taking an initial pressure measurement in the closed cell at time = zero and a final pressure measurement at some later time (typically 20 to 60 seconds). This procedure was repeated typically three times at each flow setting, and three or four flow settings were used for each calibration. The calibrated flow rate was calculated as

$$F = \left(\frac{\Delta P}{\Delta t}\right)\left(\frac{760}{60}\right)\left(\frac{T}{273}\right)(V) \qquad \textbf{(2.11)}$$

where F is in units of standard cubic centimeters per minute (sccm), P is in torr, t is in seconds, T is in Kelvin, and V is the flow cell volume in cm^3. The volume is not important to know accurately since relative flow rates were of actual interest to determine the relative proportions of the gas species present in the flow photolysis cell. Partial pressures (P_i) of each of the gases in an experiment were determined from the flow rates of each of the gases (F_i), the total flow rate ($F_t = \Sigma F_i$) and the total gas pressure (P_t) as follows:

$$P_i = (F_i / F_t)(P_t) \quad \textbf{(2.12)}$$

The factors, (760/60)(T/273)V, in equation 2.6 cancel in the flow rate ratio of equation 2.7 so that the quantity, ΔP/Δt, may be used as a relative flow rate value for each of the gases. More commonly, these ΔP/Δt relative flow rate values are used rather than calculating the flow rates in sccm. From the calibration data for each gas, a plot of ΔP/Δt vs. flow rate setting were subjected to a linear regression so that relative flow rates could be calculated for any flow rate setting. Concentrations of the gases (N_i) in units of molecules/cm^3 were then calculated by

$$N_i = (9.66x10^{18})P_i / T \quad \textbf{(2.13)}$$

Targeted values for gas flow rates were determined from the desired partial pressures of the gases for each experiment and from the requirement that the linear flow velocity of gases through the cell be ≥ 10 cm/s in order to present a fresh gas mix to the photolysis region for each laser shot.

4. Detector and Filters

An Infrared Associates mercury-cadmium-telluride detector with a 4 mm x 4mm active area was used in all experiments. This detector was equipped with a ZnSe window and a ZnSe internal lens to enhance the light gathering efficiency. The detector response in the 3-19 μm wavelength region is presented in Figure 2.2.

The detector is supported within a Dewar and filled with liquid nitrogen (77 K) during operation. The basic principle of operation is the decrease in electrical resistance when exposed to infrared radiation, thereby acting as a photoresistor. It was placed into an electric circuit with a series resistance, and the voltage drop across the detector element was connected to a preamplifier. A ±15V rechargeable Ni-Cd battery pack or a ±12V rechargeable lead acid gel cell was used to provide the bias current for the detector and to power the preamplifier circuit. As such, the detector was only powered during experiments and after being filled with liquid nitrogen. Increased fluorescence incident to the detector resulted in decreased resistance and a voltage drop to the preamplifier.

Interference filters were used with this detector to transmit the vibrational emission band of interest and to eliminate background noise from outside sources, such as scattered light. The wavelength selection of these filters for specific infrared bands allowed for the transmission of the CH_4 and CD_4 emissions of interest. These filters were purchased from Optical Coatings Laboratory, Inc. (OCLI) or from the Infrared Multilayer Laboratory at the University of Reading (IML) in England. For the CH_4 experiments, IML filter 24R was used. For the CD_4 experiments, IML filter 24U was used alone. The filter transmission curves are shown in Figure 2.3. Superimposed on each of these transmission curves is the respective CH_4 or CD_4 absorption spectrum in the region of the ν_4 asymmetric bending mode.

5. Oscilloscope

The data from the detector preamplifier output was collected using a LeCroy 9400 digital oscilloscope. The oscilloscope trigger was provided by a photodiode in the optics chamber upon laser firing. The analog signals from the detector were digitized typically into 2500 points per waveform and averaged over 5000 shots. The first fifth of each waveform (20%) was pre-trigger data, providing ~ 300 K background (zero) fluorescence intensity. The signal averaging acted to increase the signal while reducing noise interference. Background data with the laser beam blocked was collected for the same number of laser shots in the same time frame of the data collection with the same number of points. This was done in an effort to eliminate additional noise from 60 Hz and RF interference. The background data was digitized and stored in the oscilloscope memory. Signal data collected from experiments was subtracted from this stored background, resulting in a positive digitized waveform. A substantial radio frequency interference (RFI) noise spike from the laser Q-switch was found to occur frequently during the experiments. This spike interferes with the measurement of the rise time of the fluorescence signal by making the early time data unusable. Much effort was made to reduce this spike through background subtraction and through the shielding of the detector and preamplifier electronics and connections with aluminum foil. Additionally, for the later CD_4 experiments, the detector and preamplifier were housed in a specially crafted electronics box or "Faraday cage" (constructed by Alan Forlines) to suppress the RFI and electrical noise.

6. Computer/Data Reduction

The digitized experimental data from the oscilloscope was transferred to a IBM-compatible Pentium 3 computer via a RS-232 interface. The data transmitted could be of the raw data, raw background, or the background-subtracted positive waveform. The transmission of data was accomplished by a BASIC code provided by LeCroy and slightly modified in house. The data files were then converted to a text file format to be imported into SigmaPlot (version 8.02) via code in QUICKBASIC (Microsoft version 4.50). The data sets were imported into SigmaPlot, plotted, and subjected to an iterative non-linear least squares fit to a sum of exponential terms for the post trigger data. These fits provided experimental rate coefficients and pre-exponential factors for further comparison to kinetic equations derived from the supposed kinetic mechanism.

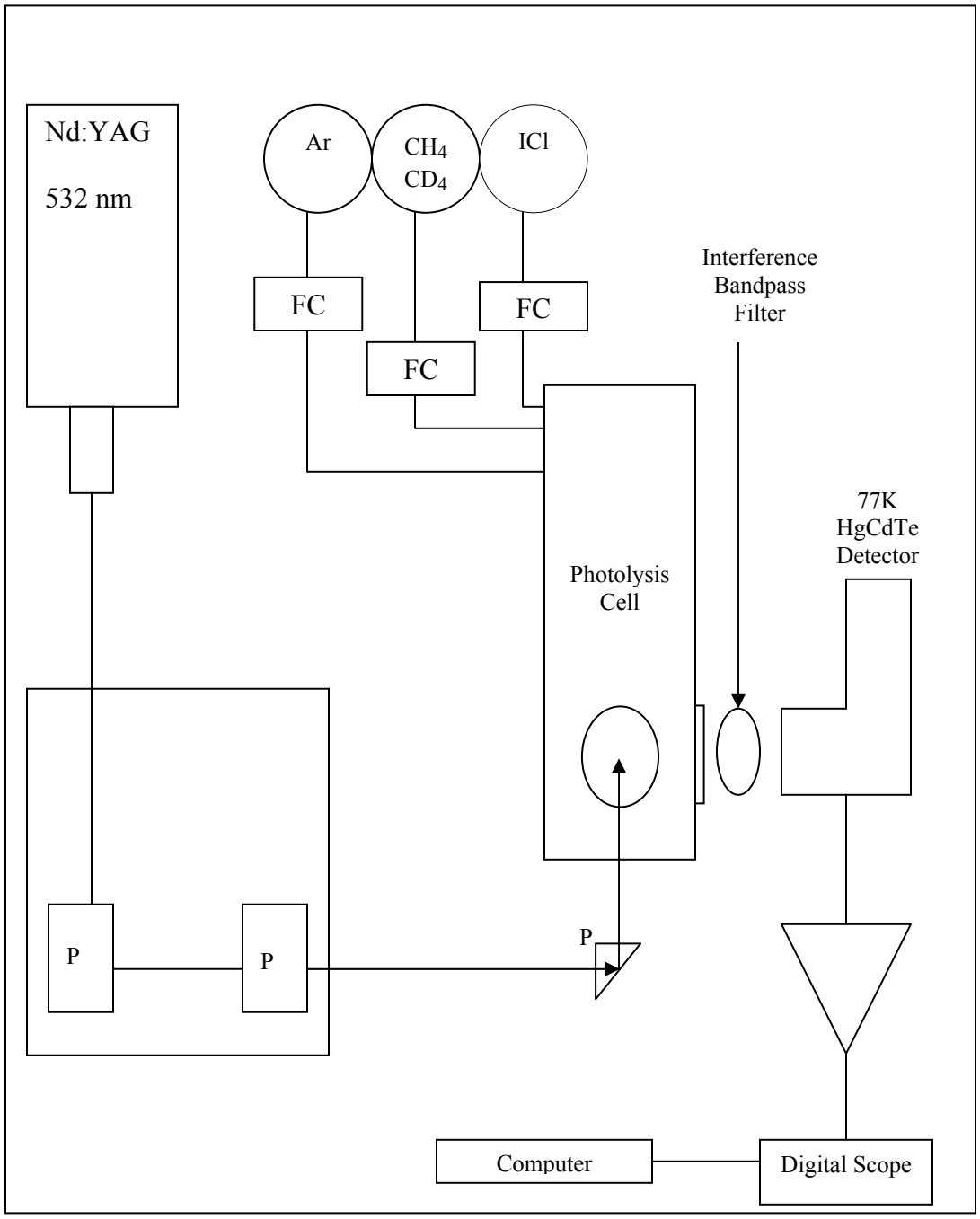

Figure 2.1 Photolysis Cell Schematic Diagram
Definition of terms: FC =Flow Controller, P = Prism

Figure 2.2: Detector Response Curve

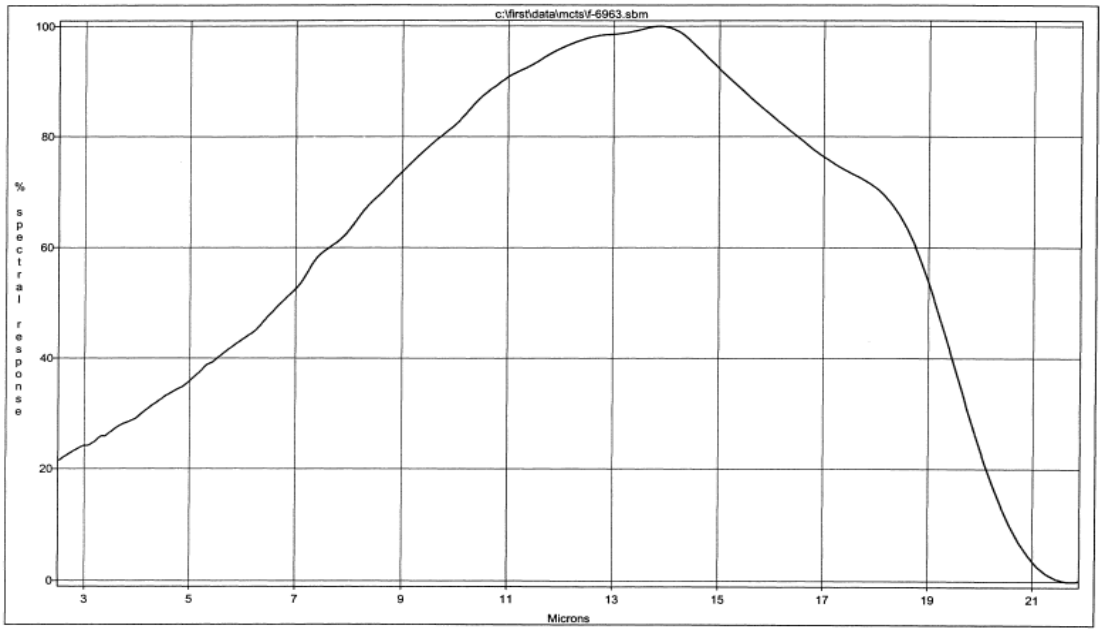

Figure 2.3: Filter Transmission Curves

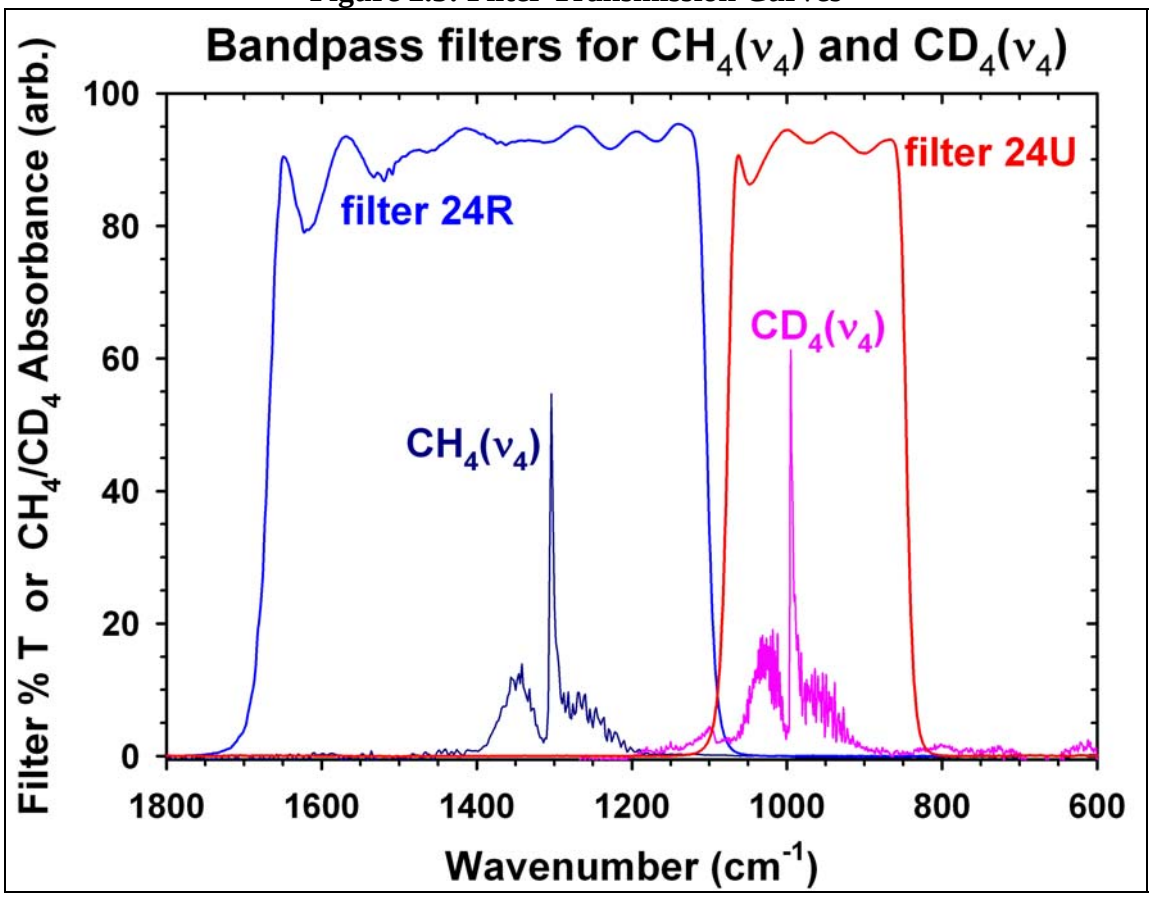

B. Chemicals

1. ICl

The iodine monochloride (ICl) used in these experiments was prepared in-house. A known mass of resublimed I_2 (Fisher ACS grade) was mixed with anhydrous calcium sulfate (Drierite®) to remove water and allowed to resublime overnight into a prepared evacuated sample tube with known mass. After the transfer was complete, the sample tube was immersed in liquid nitrogen and exposed to vacuum in an attempt to remove any air that may have entered via leaks. The sample tube was then weighed to obtain the mass of I_2 present. The stoichiometric amount of Cl_2 (Matheson HP grade, distilled) necessary to react with the known mass of I_2 in the sample tube was calculated. Successive iterations of Cl_2 additions were accomplished, and at each step the total added pressure was recorded. Once the total pressure neared the previously calculated value, the sample tube was removed, weighed, and calculations performed to determine the amount of Cl_2 necessary to achieve the correct stoichiometric ratio. One more Cl_2 addition was accomplished to reach equivalence. The resulting ICl/reactant mixture was melted for a time and allowed to sit overnight to complete the reaction and the ICl was ready for use. Stoichiometric ICl purities typically were >99.9%.

2. Gases

The argon was contained in a full size 1A cylinder purchased from Matheson (UHP grade, 99.999%), and was equipped with the appropriate two-stage regulator. The argon

was connected to the flow controller gas manifold using copper tubing and purified by passing through molecular sieve traps.

Methane was also purchased (Liquid Carbonic, 99.97% purity and 99.99% research grade from Spectra Gases) and equipped with an appropriate two-stage regulator. Similarly, deuterated methane (CD_4) was purchased in a small lecture bottle (Isotec, $\geq$ 99% d_4 purity) and connected to a flow controller. The tubing was conditioned by exposure to CD_4 for several hours. This gas was pumped away and the tubing refilled with fresh sample before experiments. No C-H stretching bands were observed by FTIR analysis of CD_4 that passed through the tubing and flow controller and was sampled from the photolysis cell.

RESULTS AND DISCUSSION

A. Kinetic Scheme

A kinetic scheme has been developed which fits the experimental observations presented in the following sections. In the process of developing this method, it was necessary to investigate several factors that could directly affect the behavior of the CH_4/CD_4 fluorescence. First, since Cl^* was not being observed directly, the possibility of CH_4/CD_4 excitation by I^* was considered. The photon energy at 532 nm is too low to create I^* from ICl or from I_2. Additionally, multiple quenching rates of I^* by CH_4 have been determined ranging from 5.9×10^{-14} to 1.1×10^{-13} cm^3 $molecule^{-1}$ s^{-1} (87). The experimentally determined average rate coefficient for Cl^* quenching by CH_4, given as 1.9×10^{-11} cm^3 $molecule^{-1}$ s^{-1}, was found to be 170 to 320 times faster (97). Although no detector was used to confirm the presence or absence of I^* in these experiments, the above factors make it unlikely that I^* was a contributing factor in the investigated E-V experiments.

A second factor considered for the kinetic scheme development was the excitation of CH_4/CD_4 via translational energy of the Cl^* or I atoms produced through photolysis. The translational energy of the Cl^* was calculated from energy and momentum conservation rules to be approximately 400 cm^{-1} (88). This calculated energy is only slightly above the average translational energy, $3kT/2 \approx 312$ cm^{-1} at room temperature. Since I is a heavier atom than Cl^*, its velocity is expected to be less than that of Cl^*. In addition, as

previously mentioned, argon gas was introduced to the reaction mixture. As stated in previously reported experimental data in the vibrational excitation of SO_2 molecules by Cl^*, argon was not effective in quenching Cl^*, but was very effective as a moderator gas to thermalize translational energy (89).

Finally, another complication could potentially arise from the formation of reaction products between CH_4/CD_4 and Cl^*. The endothermic ground state reaction between Cl and CH_4 has been found to be a slow bimolecular reaction, forming HCl and CH_3 with a rate coefficient of approximately 1 x 10^{-14} $cm^3 \cdot molecule^{-1} \cdot s^{-1}$ (79). Reactive collisions of Cl^* with hydrocarbons are generally expected to be a very minor channel due to symmetry constraints, and the limited experimental data suggests only upper limits for the reactive channels of <30% and <10% of total quenching, respectively, for methane and methane-d_4. Matsumi, *et. al.* (76) were able to show that the removal of Cl^* through a reaction pathway with CH_4 is minor ($k^*_{rxn} < 10^{-11}$ $cm^3 \cdot molecule^{-1} \cdot s^{-1}$) when compared to the collisional deactivation pathway (their rate coefficient is $k^*_Q = 3 \times 10^{-11}$ $cm^3 \cdot molecule^{-1} \cdot s^{-1}$). Their upper limit on the reactive channel was set by a complete lack of observation of reactive loss of Cl^* and a consideration of uncertainties. Deactivation of Cl^* by CH_4 through E-V pathways has been supported by the analogous efficient quenching rates observed for deactivation of Cl^* by CO_2, SF_6, H_2, and D_2, as reported by Sotnichenko, Bokun, and Nadkhin (90). These quenching rate coefficients for Cl^* were (1-15) x 10^{-11} cm^3 $molecule^{-1}$ s^{-1} as determined by direct observation of Cl^*. These rates were attributed to the deactivation by the above collision partners via near resonant energy transfer through E-V,R pathways. Experimentally determined rate coefficients for

the deactivation of Cl^* by CH_4 range from 1.9 to 3.0 x 10^{-11} cm^3 $molecule^{-1}$ s^{-1} in a recent review (87). A single measurement of (1.3 ± 0.4) x 10^{-10} cm^3 $molecule^{-1}$ s^{-1} for the deactivation of Cl^* by CD_4 also is cited (87). Both of these experimentally-determined values are consistent with the results of Cl^* deactivation by similar molecules in processes that are thought to be largely channeled through E-V or E-R,T pathways.

The proposed Cl^*/CH_4 kinetic mechanism is presented by the following process:

Cl^* formation: $ICl + h\nu \rightarrow I(^2P_{3/2}) + Cl^*(^2P_{1/2})$ **(3.1)**

Cl^* deactivation: $Cl^* + CH_4 \xrightarrow{k^*_{EV}} Cl + CH_4(\nu_4, 1306cm^{-1})$ **(3.2)**

$Cl^* + CH_4 \xrightarrow{k^*_{other}} Cl + CH_4(\nu_2, 0)$ **(3.3)**

$Cl^* + ICl \xrightarrow{k^*_{ICl}} Cl + ICl\ (or\ Cl_2 + I)$ **(3.4)**

$Cl^* \xrightarrow{k^*_o}$ *other 1st-order losses* **(3.5)**

CH_4 relaxation: $CH_4(\nu_4) \xrightarrow{k_{rad}} CH_4 + h\nu_{IR}(7.7\mu m)$ **(3.6)**

$CH_4(\nu_4) + M \xrightarrow{k^M_V} CH_4 + M$ **(3.7)**

Equation 3.1 describes the photodissociation of ICl by the laser. Equations 3.2 – 3.5 are the processes by which Cl^* can be deactivated. Two relaxation pathways of CH_4 (ν_4) are shown by equations 3.6 – 3.7. Since experimental observations were conducted under pseudo-first order conditions such that $[Cl^*] << [CH_4]$ or [ICl], the following differential equations were derived to describe the kinetics.

For the deactivation of Cl^*, the individual starred rate constants from equations 3.2 – 3.5 can be combined into a single pseudo-first order rate coefficient (k_Q):

$$\frac{-d[Cl^*]}{dt} = \left[(k^*_{EV} + k^*_{other})[CH_4] + k^*_{ICl}[ICl] + k^*_o \right] \left[Cl^* \right] \tag{3.8}$$

$$\frac{-d[Cl^*]}{dt} = k_Q[Cl^*] \tag{3.9}$$

Similarly, the formation of CH_4 (ν_4) can be represented through the following differential equation:

$$\frac{d[CH_4(\nu_4)]}{dt} = -\left(k_{rad} + \sum_M k_V^M [M] \right) \left[CH_4(\nu_4) \right] + k^*_{EV}[CH_4][Cl^*] \tag{3.10}$$

$$\frac{d[CH_4(\nu_4)]}{dt} = -k_V[CH_4(\nu_4)] + k^*_{EV}[CH_4][Cl^*] \tag{3.11}$$

where k_V is the pseudo first-order rate coefficient for all collisional deactivations of $CH_4(\nu_4)$ and it is assumed that the radiative relaxation of $CH_4(\nu_4)$ through 7.7 μm photon emission is negligible. Therefore, the differential equations given in equations 3.9 and 3.11 can be solved via a matrix approach where

$$\begin{bmatrix} \dot{\left[Cl^* \right]} \\ \dot{\left[CH_4(\nu_4) \right]} \end{bmatrix} = \begin{bmatrix} k_Q & 0 \\ k^*_{EV}[CH_4] & k_V \end{bmatrix} \begin{bmatrix} \left[Cl^* \right] \\ \left[CH_4(\nu_4) \right] \end{bmatrix} \tag{3.12}$$

The dot notation indicates time derivatives. The determinant,

$$\begin{bmatrix} k_Q - \lambda & 0 \\ k_{EV}^{*}[CH_4] & k_V - \lambda \end{bmatrix} = 0 \qquad \textbf{(3.13)}$$

can be solved to obtain two eigenvalues, λ, which are the observable rate coefficients:

$$\left(k_Q - \lambda\right)\ \left(k_V - \lambda\right) = 0 \qquad \textbf{(3.14)}$$

The solutions are

$$\lambda = k_Q \ \textit{and}\ \lambda = k_V\textbf{,} \qquad \textbf{(3.15)}$$

and the bend-excited methane population is:

$$[CH_4(\nu_4)]_t = a_1 e^{-k_Q t} + a_2 e^{-k_V t} \qquad \textbf{(3.16)}$$

where a_1 and a_2 are pre-exponential coefficients.

From equation 3.9,

$$[Cl^*]_t = [Cl^*]_0 e^{-k_Q t} \qquad \textbf{(3.17)}$$

where the initial Cl^* concentration can be estimated using Beer's Law and Planck's Law. At t = 0, equation 3.16 can be written as:

$$0 = a_1 e^{-k_Q t} + a_2 e^{-k_V t} = a_1 + a_2 \qquad \textbf{(3.18)}$$

$$a_1 = -a_2 \qquad \textbf{(3.19)}$$

Therefore, with a_1 written simply as a, equation 3.16 may be written as:

$$[CH_4(\nu_4)]_t = a(e^{-k_Q t} - e^{-k_V t}) \qquad \textbf{(3.20)}$$

The time derivative of $[CH_4(\nu_4)]$ may be written from equation 3.11, substituting 3.20 for $[CH_4(\nu_4)]$ as:

$$\frac{d[CH_4(\nu_4)]}{dt} = -k_V a(e^{-k_Q t} + e^{-k_V t}) + k^*_{EV}[CH_4][Cl^*]_0 e^{-k_Q t} \quad \textbf{(3.21a)}$$

The time derivative of equation 3.20, directly, is:

$$\frac{d[CH_4(\nu_4)]}{dt} = -k_q a e^{-k_Q t} + k_\nu a e^{-k_\nu t} \quad \textbf{(3.21b)}$$

To solve for a, the pre-exponential coefficient, we equate the coefficients of the $e^{-k_Q t}$ terms in equations 3.21a and 3.21b as:

$$-ak_Q = ak_V + k^*_{EV}[CH_4][Cl^*]_0 \quad \textbf{(3.22)}$$

Solving for a yields:

$$a = \frac{k^*_{EV}[CH_4][Cl^*]_0}{k_V - k_Q} \quad \textbf{(3.23)}$$

Using this expression for a in equation 3.20 yields a time-dependent expression for $[CH_4(\nu_4)]$:

$$[CH_4(\nu_4)] = \frac{k^*_{EV}[CH_4][Cl^*]_0}{k_V - k_Q}\left(e^{-k_Q t} - e^{-k_V t}\right) \quad \textbf{(3.24)}$$

For the experimental system, it is expected to operate under conditions where $k_Q > k_V$, so that we may rewrite equation 3.24 as

$$[CH_4(\nu_4)] = \frac{k^*_{EV}[CH_4][Cl^*]_0}{k_Q - k_V}\left(e^{-k_V t} - e^{-k_Q t}\right) \quad \textbf{(3.25)}$$

in order that the pre-exponential factor takes a positive sign. The $e^{-k_V t}$ term describes the decay of the bend-excited methane population and the $e^{-k_Q t}$ term describes the rise.

B. Cl^* Quenching by CH_4

The total quenching rate of Cl^* by CH_4 has been determined from three sets of laboratory experiments. Previous laboratory work conducted by this group (91) has experimentally determined that the rate coefficient for Cl^* quenching by CH_4 is $k = (1.9 \pm 0.4) \times 10^{-11}$ cm^3 $molecule^{-1}$ s^{-1} ($\pm 2\sigma$). These three experimental sets serve to replicate the previously determined value. The present work also measures the branching ratio, which is the fraction of quenching collisions that result in $CH_4(\nu_4)$ excitation. Each of these experiments was conducted in a slow flow cell with an observation time of 80-160 μs. A time-resolved infrared fluorescence signal of the $CH_4(\nu_4)$ bend from these experiments is shown in Figure 3.1. The observed fluorescence shows two distinct time constants. The signal has one fast exponential rise followed by a relatively slow exponential decay. In all experiments, the first 20% of the time window examined consisted of a pre-trigger signal in order to establish the zero level response of the detector.

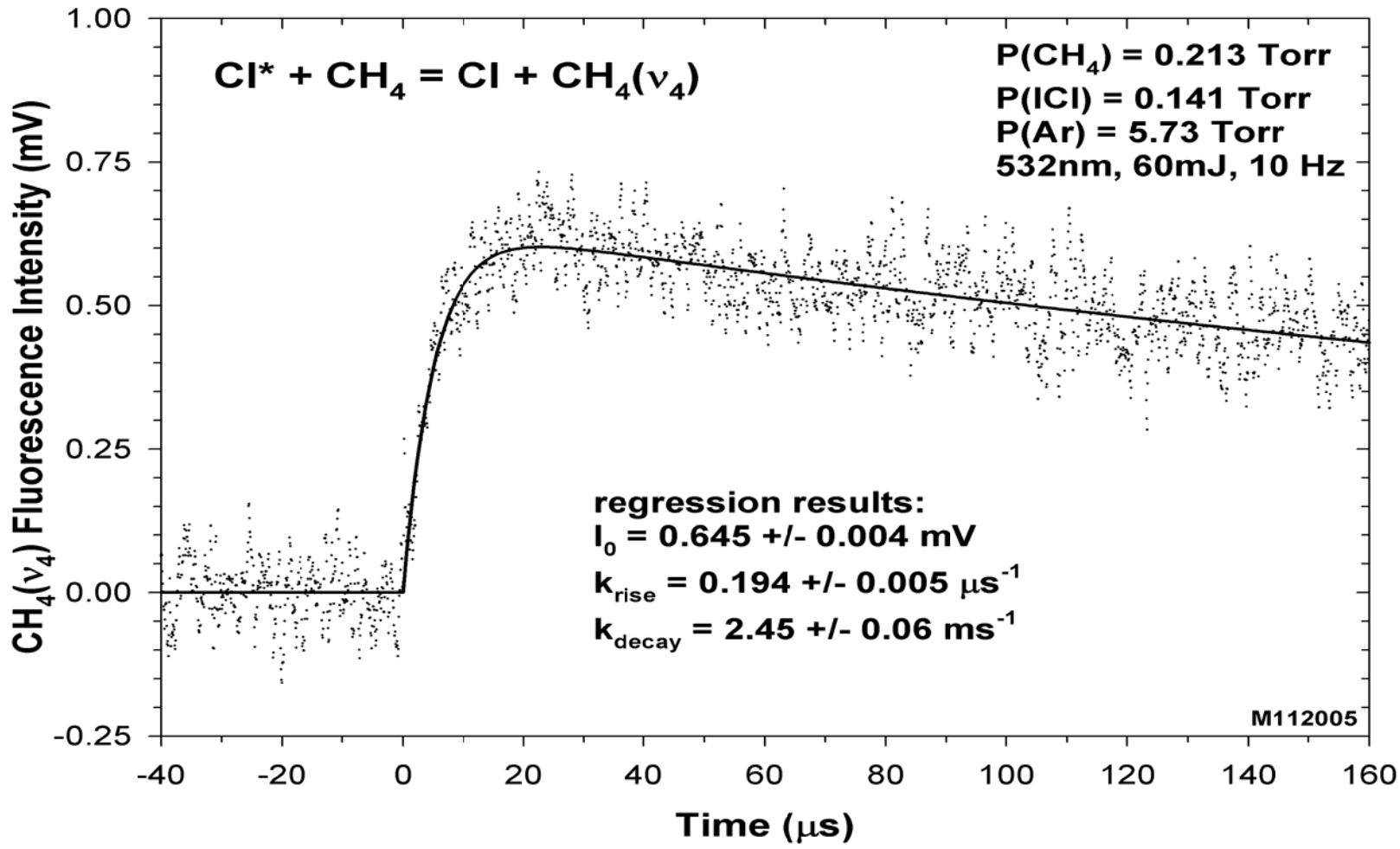

Figure 3.1: Infrared Fluorescence Signal Resulting from E-V Transfer from Cl^* to $CH_4(\nu_4)$

The assignment of Cl^* quenching to the fluorescence rise and $CH_4(\nu_4)$ relaxation to the decay is supported by the existing experimental evidence, which suggests that the quenching probability is of the order of 0.1 per collision (87) whereas methane V-T,R relaxation occurs with a much smaller probability of 0.8-2 x 10^{-5} (96, 97). Because our primary concern is the quenching rate and because it is much faster than the V-T,R relaxation, these observations follow the ν_4 fluorescence only to ≤ 40% of one natural lifetime (≤ 30% intensity loss). The resulting uncertainty in the vibrational relaxation rate coefficient is correspondingly large due to the relatively shorter observation time of the decay.

The $CH_4(\nu_4)$ bend data was found to be suitable for a non-linear least-squares fit to

$$I_f(\nu_4) = I_0(e^{-k_{decay}t} - e^{-k_{rise}t}) \qquad \textbf{(3.26)}$$

where

$$I_0 \propto \frac{k_{EV}[CH_4]}{k_Q - k_V}. \qquad \textbf{(3.27)}$$

The exponential rise and decay time constant data from these three sets of experiments are summarized in Table 3.1. The overall ICl concentrations were maintained at 0.14 to 0.15 torr and the CH_4 concentrations varied from 0.08 to 0.42 torr.

Table 3.1: Summary of $Cl^*/CH_4(\nu_4)$ Experimental Time Constant Data

Run #	P_{ICl} (torr)	P_{CH_4} (torr)	P_{Ar} (torr)	k_{rise} $(\mu s^{-1})^a$	k_{decay} $(ms^{-1})^a$
			Experimental Set #1		
1	0.141	0.103	5.756	0.1022 ± 0.0037	2.183 ± 0.039
2	0.141	0.207	5.756	0.1746 ± 0.0051	2.735 ± 0.077
3	0.141	0.311	5.756	0.2318 ± 0.0082	2.569 ± 0.079
4	0.141	0.414	5.756	0.275 ± 0.010	3.140 ± 0.080
			Experimental Set #2		
1	0.141	0.125	5.733	0.1269 ± 0.0035	2.350 ± 0.083
2	0.141	0.213	5.733	0.1935 ± 0.0051	2.451 ± 0.064
3	0.141	0.301	5.733	0.2257 ± 0.0064	3.111 ± 0.067
4	0.141	0.419	5.733	0.328 ± 0.011	3.142 ± 0.064
5	0.141	0.419	5.733	0.344 ± 0.012	2.807 ± 0.066
			Experimental Set #3		
1	0.147	0.080	2.773	0.0768 ± 0.0024	1.50 ± 0.32
2	0.147	0.160	2.773	0.1635 ± 0.0046	NM[b]
3	0.147	0.240	2.773	0.1957 ± 0.0054	1.868 ± 0.065
4	0.147	0.321	2.773	0.2485 ± 0.0068	NM[b]
5	0.147	0.401	2.773	0.2834 ± 0.0071	2.73 ± 0.13

a) Quoted errors in k_{rise} and k_{decay} are 1 standard error from the regression
b) k_{decay} values were "not measured" when the decay was too slow for accurate measurement

Figures 3.2 through 3.4 give the plots of the $CH_4(\nu_4)$ pseudo first-order rates of the exponential rises and decays versus the concentration of CH_4. Linear regressions of these data yield best-fit slopes that provide the Cl^* deactivation and $CH_4(\nu_4)$ relaxation rate coefficients.

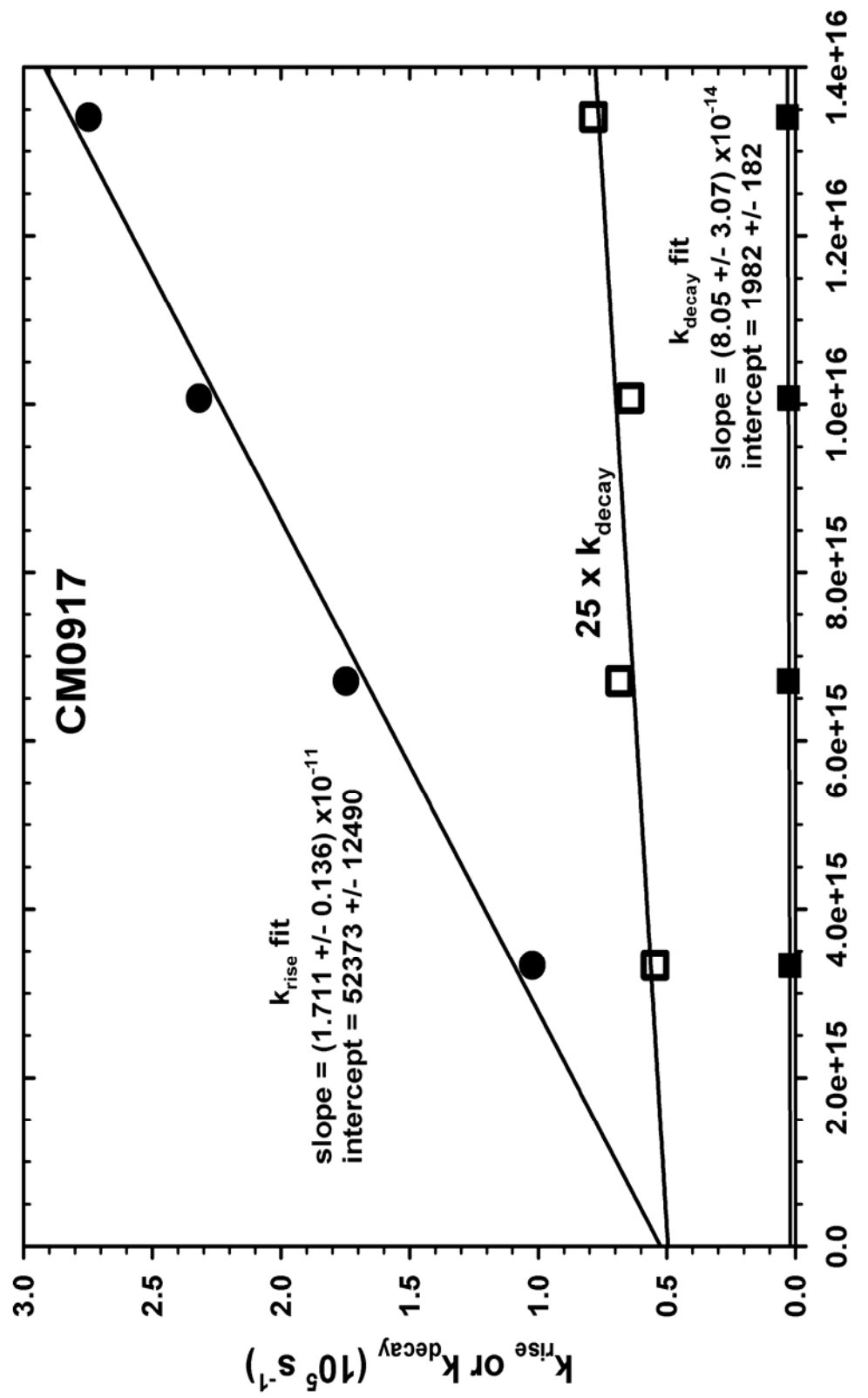

Figure 3.2: Kinetic Plot for the Total Quenching of Cl* by Methane (Experimental Set #1)

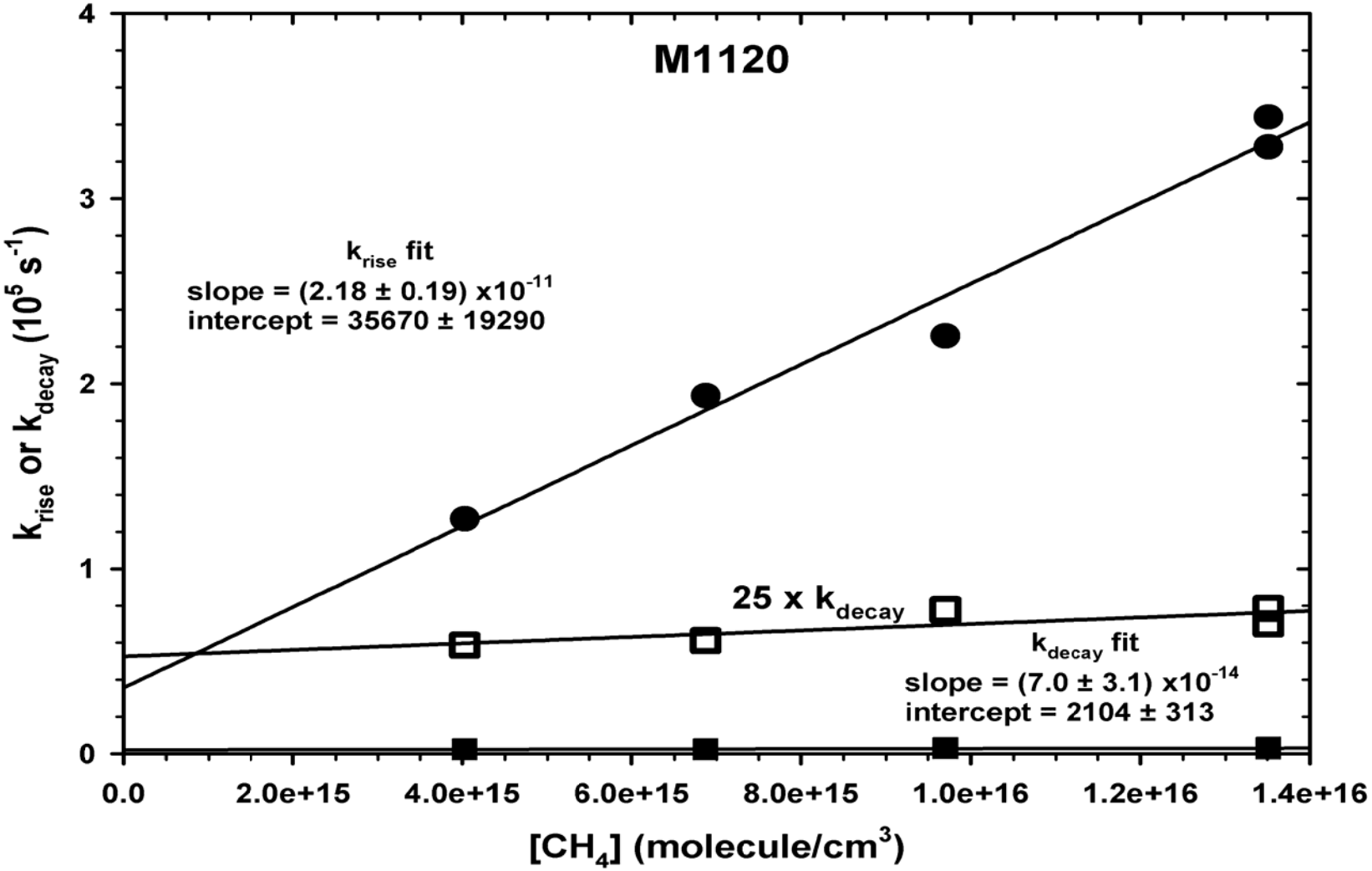

Figure 3.3: Kinetic Plot for the Total Quenching of Cl* by Methane (Experimental Set #2)

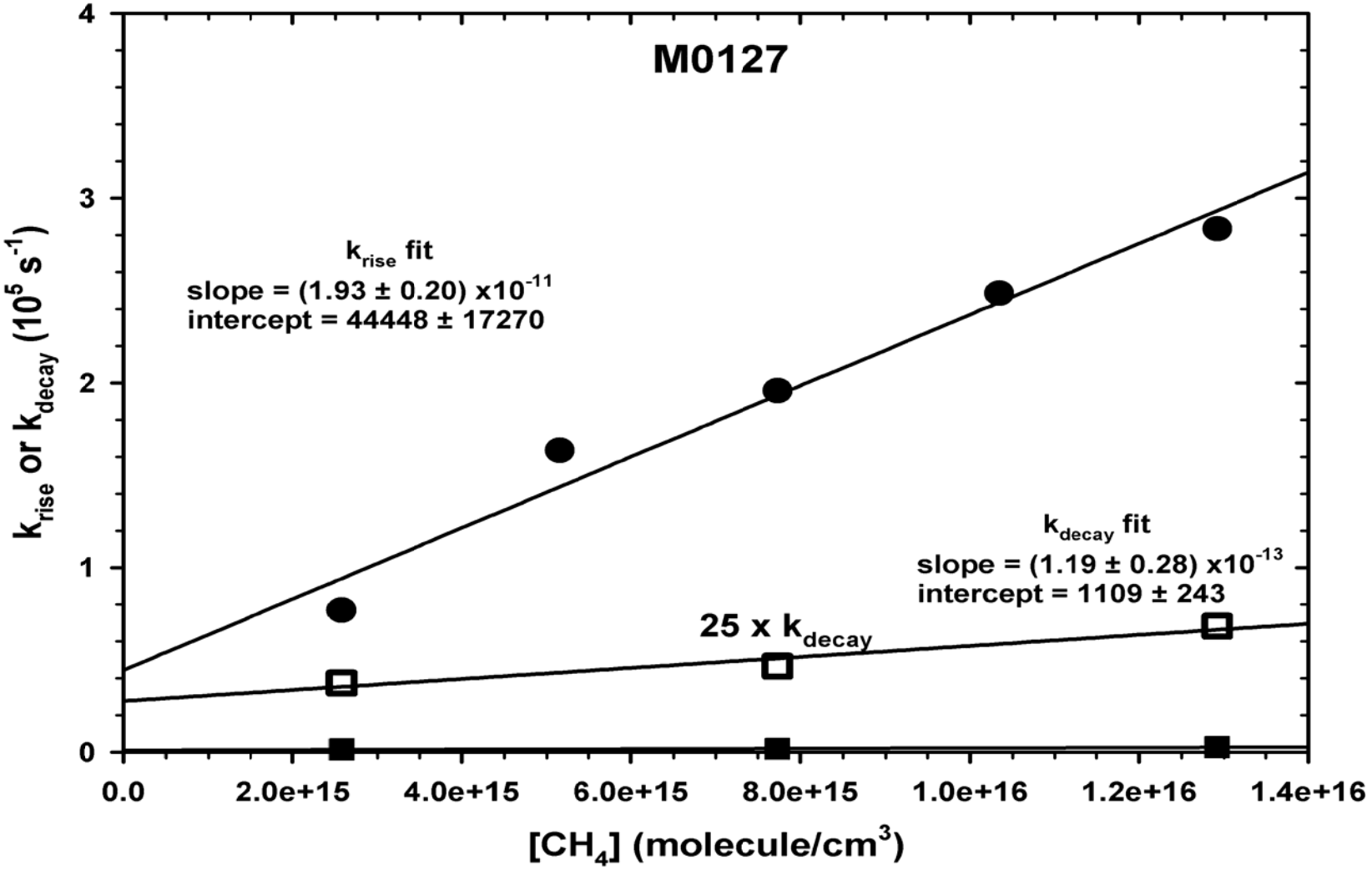

Figure 3.4: Kinetic Plot for the Total Quenching of Cl* by Methane (Experimental Set #3)

Kinetic results from the plots in Figures 3.2 - 3.4 are summarized in Table 3.2 below. The experimental rate coefficients for the total Cl^* deactivation by methane are in good agreement with each other, and the standard errors from their respective linear regressions are of the order of 10%. The average value of the Cl^* quenching rate coefficient from these three measurements was $(1.9 \pm 0.5) \times 10^{-11}$ cm^3 $molecule^{-1}$ s^{-1} and the average value of the $CH_4(\nu_4)$ V-T,R relaxation rate coefficients from these three measurements was $(9 \pm 5) \times 10^{-14}$ cm^3 $molecule^{-1}$ s^{-1}, as shown in Table 3.2, where the quoted uncertainties here are two standard deviations about the mean.

Table 3.2: Summary and Average $Cl^*/CH_4(\nu_4)$ Rate Coefficients

Experimental Set #	k_Q[a,c,d]	k_V[b,c,d]
1	1.7 ± 0.1	8.1 ± 3.1
2	2.2 ± 0.2	7.0 ± 3.1
3	1.9 ± 0.2	11.9 ± 2.8
Average	1.9 ± 0.5 $(\pm 2\sigma)$	9 ± 5 $(\pm 2\sigma)$

a) Rate coefficient for Cl^* quenching in units of 10^{-11} cm^3 $molecule^{-1}$ s^{-1}
b) Rate coefficient for $CH_4(\nu_4)$ relaxation in units of 10^{-14} cm^3 $molecule^{-1}$ s^{-1}
c) Quoted errors in expt'l k_Q and k_V are 1 standard error from the regression
d) Quoted errors in average k_Q and k_V are 2 standard deviations about the mean

A summary of experimental quenching rate coefficients obtained by different investigative methods has been made by Chichinin (87). The reported coefficients of $(2.2 \pm 0.3) \times 10^{-11}$ $cm^3 \cdot molecule^{-1} \cdot s^{-1}$ (by atomic resonance fluorescence in the vacuum ultraviolet), $(3.0 \pm 0.3) \times 10^{-11}$ $cm^3 \cdot molecule^{-1} \cdot s^{-1}$ (by laser-induced fluorescence in the vacuum ultraviolet), and $(1.9 \pm 0.6) \times 10^{-11}$ $cm^3 \cdot molecule^{-1} \cdot s^{-1}$ (by time-resolved laser magnetic resonance) are in good agreement with the measured value reported in this work. Furthermore, Bartell's (91) quenching rate coefficient of $(1.9 \pm 0.4) \times 10^{-11}$

$cm^3 \cdot molecule^{-1} \cdot s^{-1}$ ($\pm 2\sigma$) from similar experiments is in excellent agreement with the results obtained in this work.

C. Cl^* Quenching by CD_4

The Cl^*/CD_4 E-V process has a smaller ΔE (114 cm^{-1}) than the Cl^*/CH_4 process (ΔE = 424 cm^{-1}) The ν_4 asymmetric bending frequency is reduced from 1306 cm^{-1} in methane to 996 cm^{-1} in methane-d_4 (94). A common theme of the theoretical treatments of E-V transfer is that the probability of E-V transfer in the quenching of X^* species by small molecules is increased when the ΔE is small for the E-V process described in reaction 1.5 (21,56,87). Therefore, the E-V transfer is expected to be efficient when the Cl^* electronic excitation energy is near to that of a small molecule's vibrational normal mode and when the IR fundamental absorption band is strong. This justification predicts that the Cl^*/CD_4 quenching rate coefficient should be larger than that of the Cl^*/CH_4 system. Further, because the CD_4 vibrational level is nearer to the Cl^* energy, it is predictable that a larger fraction of the Cl^*/CD_4 quenching collisions should follow the E-V excitation pathway compared to the E-V fraction of Cl^*/CH_4 quenching (to a higher energy, less accessible, bending vibration). This prediction will be assessed in a later section.

Four sets of experiments were conducted in which total quenching of Cl^* by CD_4 was investigated. Similar conditions and procedures, as described in the preceding section for CH_4, were employed in these experiments with CD_4. The overall ICl concentrations were maintained in the narrow range 0.12 to 0.15 torr and the CD_4 concentrations were varied

from 0.03 to 0.12 torr. Argon pressures between 2 and 3 torr served to thermalize Cl^* atoms from the photolysis event.

Figure 3.5 shows a time- resolved infrared fluorescence signal of the $CD_4(\nu_4)$ bend following E-V transfer from Cl^*. On the faster time scales necessary to capture the fluorescence rise, the fluorescence decay is too slow and too noisy for reliable measurements within the selected observation period. Nonetheless, in order to obtain suitable k_{rise} values from the data, all $CD_4(\nu_4)$ fluorescence signals were fitted to a difference of exponential terms as in Equation 3.26. Decay rates ranged from zero to a few ms^{-1}, but they were not reliably proportional to CD_4 concentrations and do not yield useful kinetic plots. Accordingly, no kinetic plots of the decay data sets are presented. The pseudo first-order exponential rates of fluorescence rise and decay from the four sets of experiments are summarized in Table 3.3. Quoted errors in k_{rise} and k_{decay} values are 1 standard error from the regression. Figures 3.6 through 3.9 present the kinetic plots of the $CD_4(\nu_4)$ pseudo first-order exponential rates of fluorescence rise versus the concentration of CD_4.

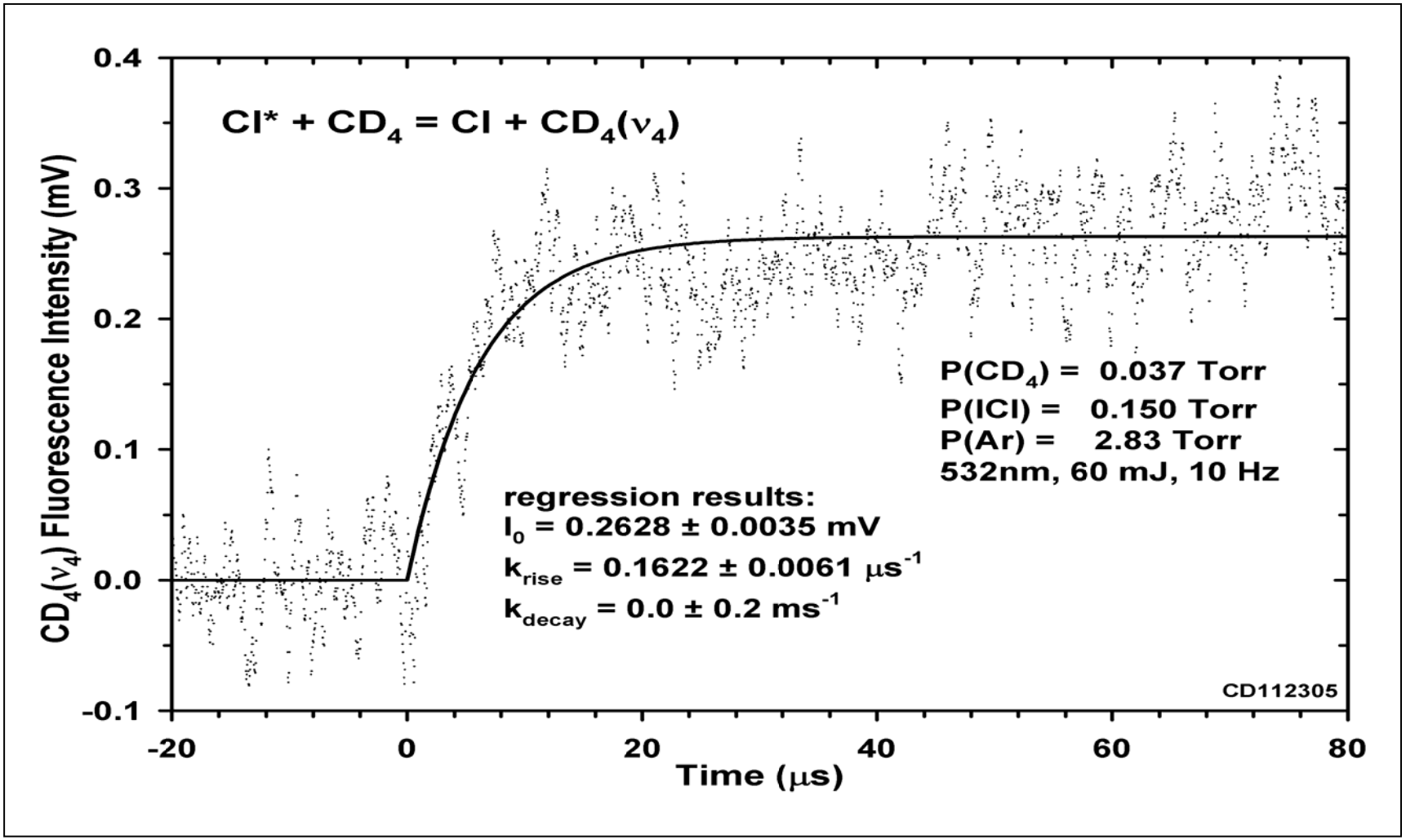

Figure 3.5: Infrared Fluorescence Signal resulting from E-V Transfer from Cl^* to $CD_4(\nu_4)$

Table 3.3: Summary of Cl*/$CD_4(\nu_4)$ Experimental Time Constant Data

Run #	P_{ICl} (torr)	P_{CD_4} (torr)	P_{Ar} (torr)	$k_{rise}\ (\mu s^{-1})^a$	$k_{decay}\ (ms^{-1})^{a,b}$
			Experimental Set #1		
1	0.1248	0.0253	2.362	0.345 ± 0.034	0.0 ± 0.2
2	0.1248	0.0377	2.362	0.235 ± 0.035	4.10 ± 0.46
3	0.1248	0.0377	2.362	0.325 ± 0.030	2.80 ± 0.22
4	0.1248	0.0626	2.362	0.545 ± 0.068	1.47 ± 0.23
5	0.1248	0.0626	2.362	0.658 ± 0.081	0.0 ± 0.2
6	0.1248	0.0751	2.362	0.648 ± 0.090	1.82 ± 0.23
			Experimental Set #2		
1	0.1302	0.0129	2.457	0.0925 ± 0.0076	5.4 ± 0.9
2	0.1302	0.0260	2.457	0.1823 ± 0.0087	1.4 ± 0.3
3	0.1302	0.0260	2.457	0.239 ± 0.012	0.5 ± 0.3
4	0.1302	0.0390	2.457	0.1458 ± 0.0069	5.7 ± 0.4
5	0.1302	0.0520	2.457	0.4560 ± 0.0020	0.7 ± 0.2
6	0.1302	0.0651	2.457	0.323 ± 0.020	1.7 ± 0.3
7	0.1302	0.0651	2.457	0.686 ± 0.047	0.7 ± 0.2
8	0.1302	0.0781	2.457	0.556 ± 0.031	2.6 ± 0.2
			Experimental Set #3		
1	0.1306	0.0167	2.453	0.1001 ± 0.0063	0.0 ± 0.5
2	0.1306	0.0331	2.453	0.2026 ± 0.0076	0.0 ± 0.2
3	0.1306	0.0331	2.453	0.231 ± 0.012	1.8 ± 0.3
4	0.1306	0.0496	2.453	0.336 ± 0.020	0.0 ± 0.3
5	0.1306	0.0660	2.453	0.402 ± 0.026	0.0 ± 0.3
6	0.1306	0.0824	2.453	0.339 ± 0.014	3.8 ± 0.2
7	0.1306	0.0824	2.453	0.356 ± 0.018	1.4 ± 0.2
8	0.1306	0.0989	2.453	0.486 ± 0.023	0.0 ± 0.2
9	0.1306	0.0989	2.453	0.676 ± 0.058	0.7 ± 0.3
10	0.1306	0.1153	2.453	0.394 ± 0.022	2.3 ± 0.2
11	0.1306	0.1153	2.453	0.423 ± 0.026	0.3 ± 0.2
			Experimental Set #4		
1	0.1503	0.0181	2.832	0.1093 ± 0.0049	2.4 ± 0.4
2	0.1503	0.0368	2.832	0.1622 ± 0.0061	0.0 ± 0.2
3	0.1503	0.0555	2.832	0.328 ± 0.015	1.2 ± 0.2
4	0.1503	0.0742	2.832	0.324 ± 0.016	1.4 ± 0.2
5	0.1503	0.0929	2.832	0.396 ± 0.020	1.2 ± 0.2
6	0.1503	0.0929	2.832	0.527 ± 0.031	2.1 ± 0.2
7	0.1503	0.1116	2.832	0.388 ± 0.019	0.0 ± 0.2

a) Quoted errors are 1 standard error from the regression

b) k_{decay} values are listed for completeness, but they do not support a valid determination of a vibrational relaxation rate coefficient

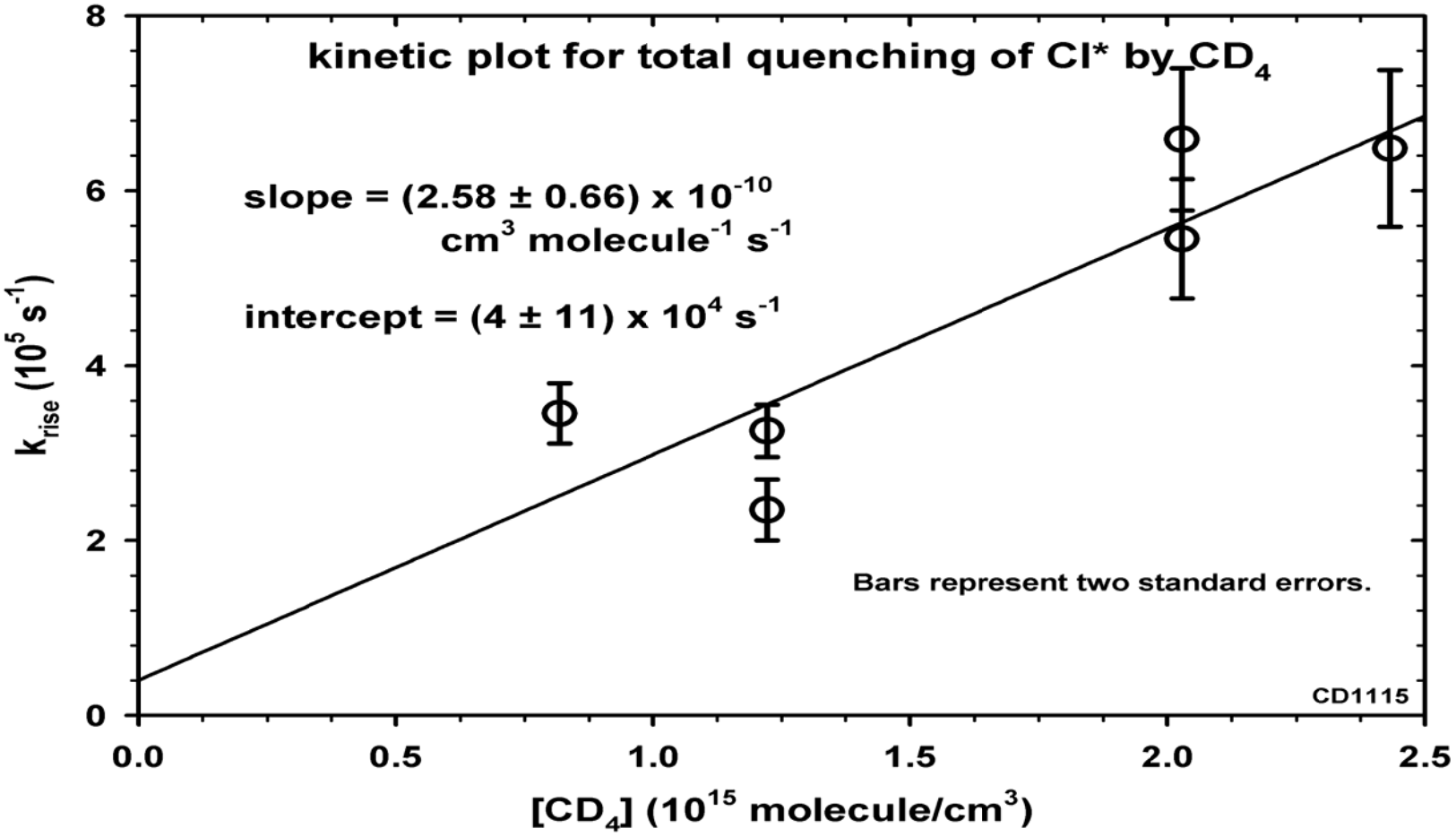

Figure 3.6: Kinetic Plot for the Total Quenching of Cl* by Methane-d_4 Concentration (Experimental Set #1)

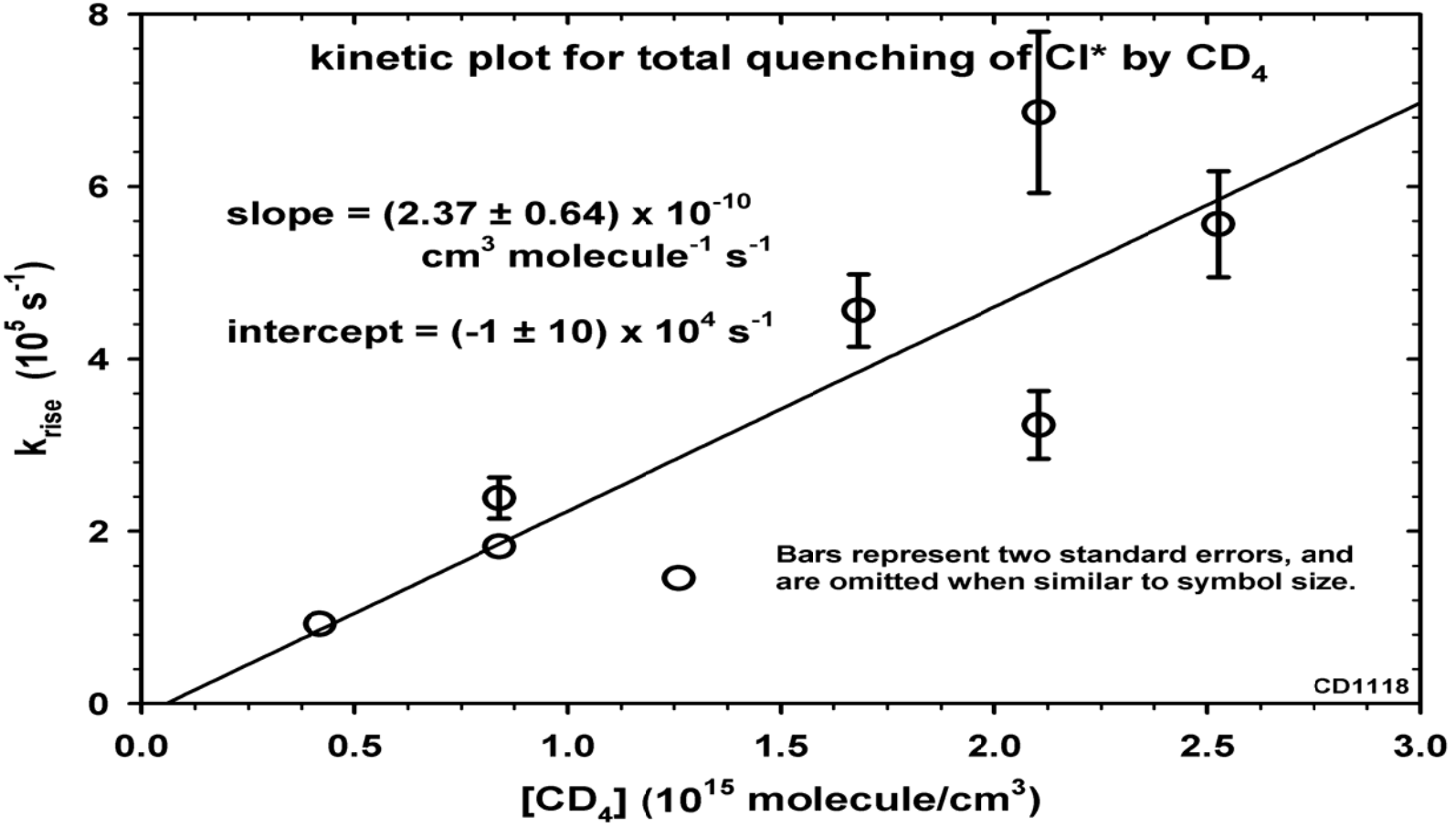

Figure 3.7: Kinetic Plot for the Total Quenching of Cl* by Methane-d_4 Concentration (Experimental Set #2)

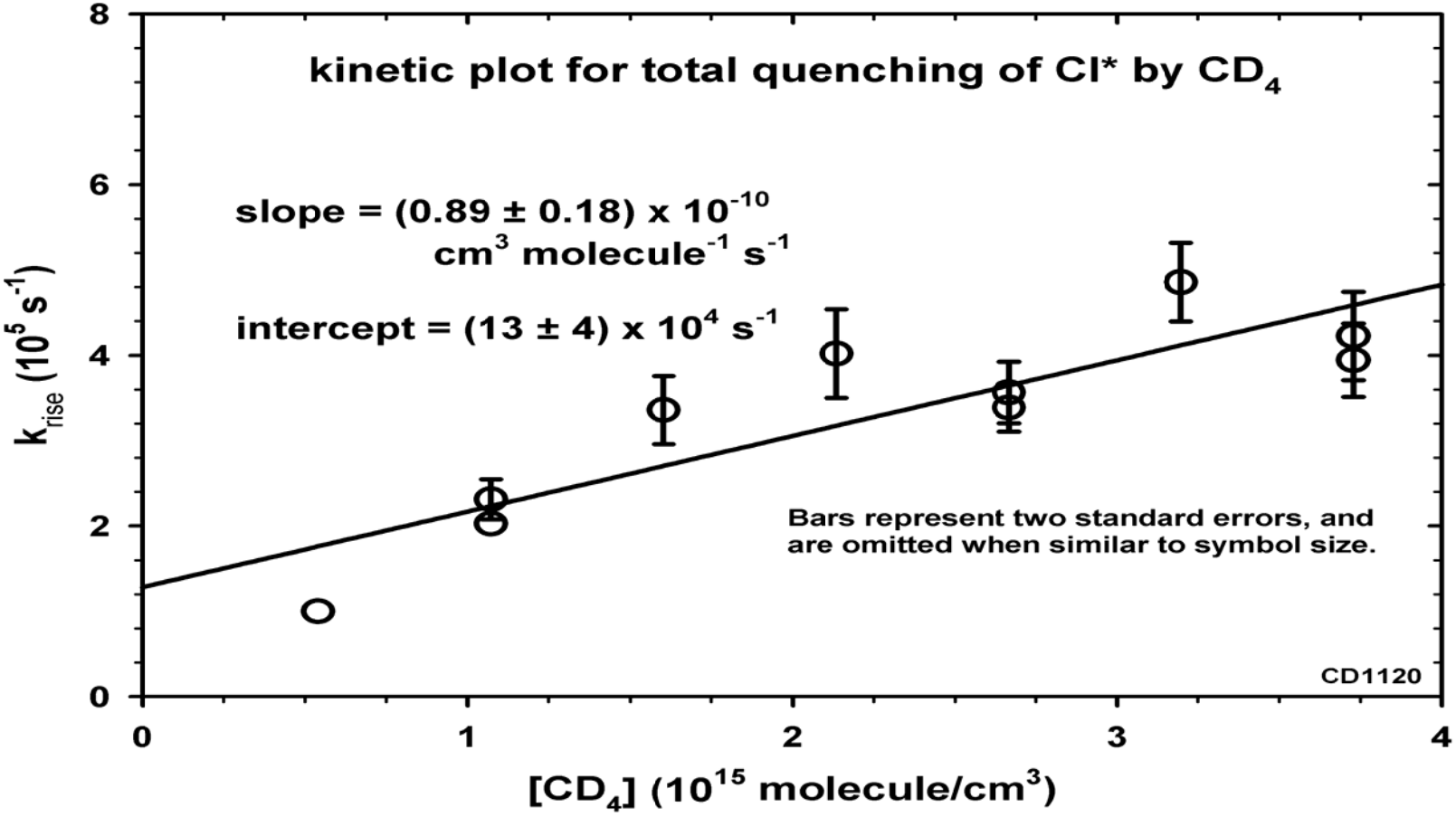

Figure 3.8: Kinetic Plot for the Total Quenching of Cl* by Methane-d_4 Concentration (Experimental Set #3)

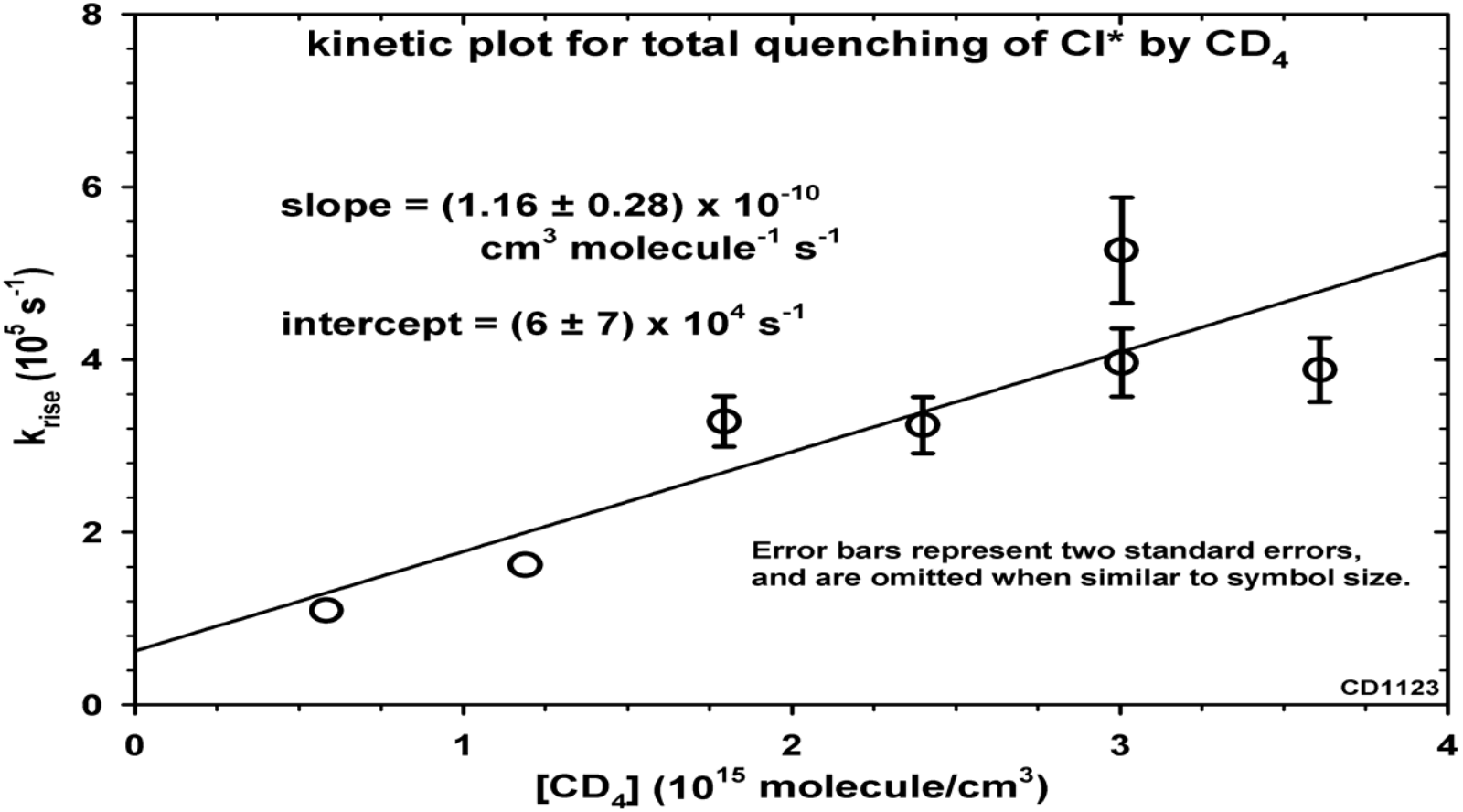

Figure 3.9: Kinetic Plot for the Total Quenching of Cl* by Methane-d_4 Concentration (Experimental Set #4)

Best fit slopes from linear regressions of the data plotted in Figures 3.6-3.9 provide the Cl^* deactivation rate coefficients reported in Table 3.4. There is nearly a factor of three scatter in the rate coefficients determined in these experiments. This is not a desirable situation; however, the signal-to-noise ratios in these observations are very low even after 5000 shots of data collection. The weighted average value of the Cl^* quenching rate coefficient was $(1.4 \pm 0.9) \times 10^{-10}$ cm^3 molecule^{-1} s^{-1}, where the stated uncertainty is two standard deviations about the weighted mean. As predicted above, this rate coefficient is larger than the Cl^*/CH_4 quenching rate coefficient by about a factor of 7. The Cl^*/CD_4 quenching rate coefficient determined in the present work is in good agreement with Chichinin's (56) reported value of $(1.3 \pm 0.4) \times 10^{-10}$ cm^3 molecule^{-1} s^{-1}, albeit with about twice the uncertainty.

Table 3.4: Summary and Average $Cl^*/CD_4(\nu_4)$ Rate Coefficients

Experimental Set #	k_Q [a,b]
1	2.6 ± 0.7
2	2.4 ± 0.6
3	0.9 ± 0.2
4	1.2 ± 0.3
Weighted Average	1.4 ± 0.9 ($\pm 2\sigma$)[c]

a) Rate coefficient for Cl^* quenching, in units of 10^{-10} cm^3 molecule^{-1} s^{-1}
b) Quoted errors in expt'l k_Q values are ± 1 standard error from the regression
c) Quoted error in average k_Q is 2 standard deviations about the mean

As noted in Table 3.3, the $CD_4(\nu_4)$ relaxation time constant could not be measured reliably. The decay rates were very slow on the time scale of the experiments and often there was no perceptible decay of the fluorescence. As a result, the $CD_4(\nu_4)$ vibrational relaxation rate coefficient could not be accurately determined. In part, this was

aggravated by the fact that the range of CD_4 concentrations used to gather the experimental data was less than the range of CH_4 concentrations.

Brian Brumfield's 2005 MS thesis from this group (98) also provides two unpublished rate coefficient measurements for Cl^* quenching by CD_4 for comparison with the present results. Brumfield's measurements were made by observing Cl^* E-V transfer-excited fluorescence from $N_2O(\nu_1)$ or $SO_2(\nu_3)$, and measuring the increasing rate of Cl^* quenching as increasing amounts of CD_4 were added. This competitive kinetic method takes advantage of the brighter fluorescence from the N_2O and SO_2 emitters. The Cl^* quenching rate coefficient for CD_4 was determined to be $(2.6 \pm 1.3) \times 10^{-10}$ $cm^3 \cdot molecule^{-1} \cdot s^{-1}$ from the N_2O observations (Brumfield's Fig. 3-8) and $(1.8 \pm 0.6) \times 10^{-10}$ $cm^3 \cdot molecule^{-1} \cdot s^{-1}$ from the SO_2 observations (Brumfield's Fig. 3-11). In each case the stated uncertainty is two standard errors from the linear regression. The highest k_{rise} data point was omitted from Brumfield's N_2O data set in arriving at the stated rate coefficient. These results also are scattered, but do overlap within stated uncertainties with the rate coefficient determined from direct $CD_4(\nu_4)$ fluorescence observations in this work.

D. E-V Branching Ratio Determination for $Cl^*/CH_4(\nu_4)$

Experiments thus far have determined the rate coefficient for total quenching of Cl^* by CH_4/CD_4 in all pathways. In principle, one may obtain this same rate coefficient for total Cl^* quenching from kinetic observations of any "active" chemical species involved in the

Cl^* quenching process (e.g. Cl, Cl^* or $CH_4(\nu_4)$). In order to determine an absolute rate coefficient for a specific quenching channel, one must have (at least relative) concentration measurements for product species in that specific channel. Infrared fluorescence observations provide the necessary intensity measurements from which to determine an E-V branching ratio in these experiments, which is the ratio of the rate of the $Cl^* \rightarrow CH_4(\nu_4)$ electronic-to-vibrational energy transfer process to that of the total Cl^* quenching by CH_4. This ratio can be mathematically described by

$$\frac{k_{EV}^*}{k_{EV}^* + k_o^*} = \frac{k_{EV}^*}{k_Q^{CH_4}} \tag{3.28}$$

where k_{EV}^* is the rate coefficient for the $Cl^* \rightarrow CH_4(\nu_4)$ process, k_o^* is the combined rate coefficient for all other Cl^* quenching processes by CH_4, and $k_Q^{CH_4}$ is the sum of k_{EV}^* and k_o^*, and represents the total $CH_4(\nu_4)$ quenching rate coefficient, which was experimentally measured in section B of this chapter. The absolute E-V rate coefficient, k_{EV}^*, is related to the back-extrapolated $CH_4(\nu_4)$ fluorescence intensity, I_0, which was obtained from the nonlinear regression of the observed fluorescence signal to Equation 3.26 in each experiment.

$$I_0 = C\left(A \cdot T_\lambda \cdot D_\lambda\right)_{\nu_4} \frac{k_{EV}^* \left[CH_4\right]\left[Cl^*\right]_0}{\left(k_Q - k_V\right)} \tag{3.29}$$

The proportionality constants C, T_λ, D_λ, and A that make this relationship an equality include factors of light collection (C), filter transmission (T_λ), detector efficiency (D_λ) and the Einstein spontaneous emission coefficient (A) as the radiative rate coefficient for photon emission. These constants are summarized in Table 3.5. It is the light collection factor (C) that is unknown in these experiments and requires a relative intensity method.

It is most expedient to use fluorescence observations of electronically-excited bromine atoms, Br^*, produced by 532 nm photolysis of IBr, as an intensity standard. When IBr is photolyzed, Br^* is produced instantly with a quantum yield of 0.68 (49) and fluoresces at 2.713 μm with a radiative rate coefficient (Einstein A coefficient) of k_{rad} = 0.909 sec (21). The Br^* fluorescence signal, presented in Figure 3.10, decays exponentially as

$$I_{Br^*} = I_0^{Br^*} e^{-kt} \qquad \textbf{(3.30)}$$

An exponential fit of the data yields an $I_0^{Br^*}$ value in millivolts that is related by the following equation to $[Br^*]_0$, the photolytically generated concentration of Br^* at time zero.

$$I_0^{Br^*} = C\left(A \cdot T_\lambda \cdot D_\lambda\right)_{Br^*} [Br^*]_0 \qquad \textbf{(3.31)}$$

The light collection factor, C, is identical to that in Equation 3.29 as long as the detector placement does not change between experiments. Equation 3.31 may be solved for C and the result substituted into Equation 3.29 and rearranged to yield:

$$k_{EV}^{*} = \frac{I_0^{\nu_4}\left(k_Q - k_V\right)\left[Br^{*}\right]_0\left(A \cdot T_\lambda \cdot D_\lambda\right)_{Br*}}{I_0^{Br*}\left[CH_4\right]\left[Cl^{*}\right]_0\left(A \cdot T_\lambda \cdot D_\lambda\right)_{CH_4(\nu_4)}} \qquad \textbf{(3.32)}$$

The $(k_Q - k_V)$ differences in Equation 3.32 are the $(k_{rise} - k_{decay})$ differences obtained from nonlinear regression results of the bending mode fluorescence.

Table 3.5: Summary of Proportionality Constants

Species	λ(μm)	Filter ID	T_λ[c]	D_λ[c]	$A_\lambda(s^{-1})$[d]
$CH_4(\nu_4)$	7.66	24R[a]	0.93	0.614	2.5
$CD_4(\nu_4)$	10.04	24U[a]	0.90	0.821	0.88
Br*	2.713	NO2710[b]	0.56	0.232	0.909

a) University of Reading, UK, Department of Astronomy
b) Optical Coatings Laboratory, Inc.
c) from detector test sheet supplied by manufacturer
d) calculated from the method described by Yardley (23, p57-58) from published data tables (99,100)

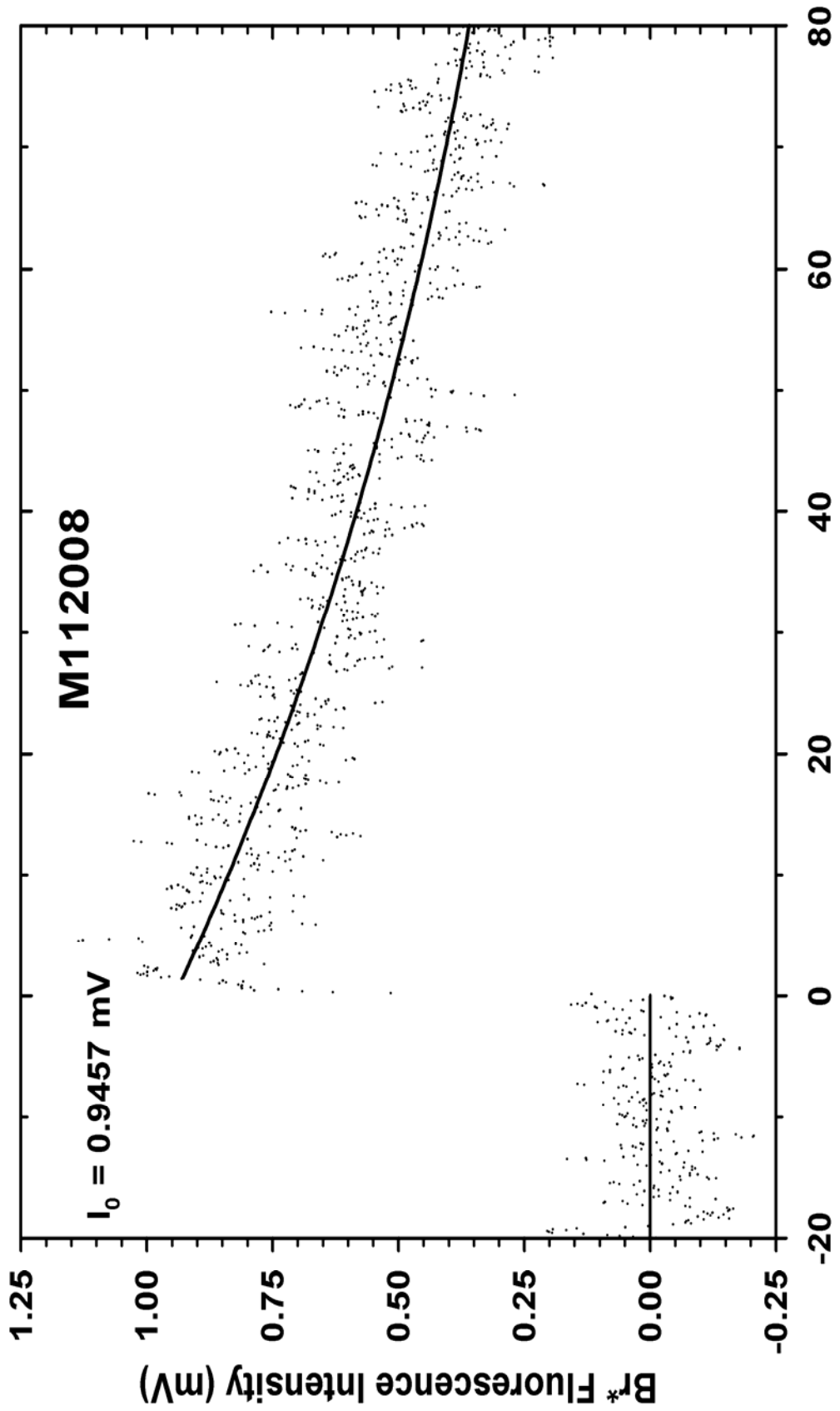

Figure 3.10: Infrared Fluorescence Signal of Br*

In both cases, $[X^*]_0$ may be calculated using the Beer-Lambert law and Planck's Law as described for Cl^* production from ICl in the experimental section. Combining these equations gives

$$k_{EV}^{*} = \frac{I_0^{\nu_4}\left(k_{rise} - k_{decay}\right)\left[Br^*\right]_0\left(A \cdot T_\lambda \cdot D_\lambda\right)_{Br*}}{I_0^{Br*}\left[CH_4\right]\left[Cl^*\right]_0\left(A \cdot T_\lambda \cdot D_\lambda\right)_{CH_4(\nu_4)}} \qquad \textbf{(3.33)}$$

The $k_{EV}^{*}/k_Q^{CH_4}$ branching ratio, given by Equation 3.28, is evaluated using experimentally derived values for both rate coefficients. The data for the E-V branching ratio evaluation in the Cl^*/CH_4 experiments are tabulated in Tables 3.6 and 3.7.

Table 3.6: Summary of Experimental Data for Cl^*/CH_4 Branching Ratio Calculation

Run #	$[Cl^*]_0$ [a] ($\times 10^{13}$)	$[Br^*]_0$ [a] ($\times 10^{14}$)	$[CH_4]$ [a] ($\times 10^{15}$)	$I_{0(CH_4(\nu_4))}$ [b]	$I_{0(Br^*)}$ [b]	$k_{rise} - k_{decay}$ (10^5 s^{-1})
			Experimental Set #1			
1	4.595	1.295	3.349	0.5505	0.5820	1.000
2	4.595	1.295	6.729	0.6015	0.5820	1.719
3	4.595	1.295	10.110	0.5559	0.5820	2.292
4	4.595	1.295	13.459	0.5615	0.5820	2.716
			Experimental Set #2			
1	4.594	2.715	4.064	0.6166	0.9457	1.246
2	4.594	2.715	6.924	0.6448	0.9457	1.911
3	4.594	2.715	9.785	0.6709	0.9457	2.226
4	4.594	2.715	13.621	0.6440	0.9457	3.248
5	4.594	2.715	13.621	0.6169	0.9457	3.413
			Experimental Set #3			
1	4.776	1.436	2.601	0.6159	0.5229	0.7530
2	4.776	1.436	5.201	0.5226	0.5229	1.635
3	4.776	1.436	7.802	0.6329	0.5229	1.938
4	4.776	1.436	10.435	0.5617	0.5229	2.485
5	4.776	1.436	13.036	0.6549	0.5229	2.807

a) Reported in units of molecules/cm^3
b) Reported in units of millivolts (mV)

Table 3.7: Cl^*/CH_4 Branching Ratio Data

Run #	k_{EV}^* (10^{-12} $cm^3 \cdot molecule^{-1} \cdot s^{-1}$)	k_Q^* [a] (10^{-11} $cm^3 \cdot molecule^{-1} \cdot s^{-1}$)	Branching Ratio
		Experimental Set #1	
1	6.39	1.7 ± 0.1	0.376
2	5.98	1.7 ± 0.1	0.352
3	4.91	1.7 ± 0.1	0.289
4	4.40	1.7 ± 0.1	0.259
		Experimental Set #2	
1	5.15	2.2 ± 0.2	0.234
2	4.85	2.2 ± 0.2	0.220
3	4.16	2.2 ± 0.2	0.189
4	4.19	2.2 ± 0.2	0.191
5	4.22	2.2 ± 0.2	0.192
		Experimental Set #3	
1	4.86	1.9 ± 0.2	0.256
2	4.47	1.9 ± 0.2	0.235
3	4.28	1.9 ± 0.2	0.225
4	3.65	1.9 ± 0.2	0.192
5	3.84	1.9 ± 0.2	0.202
Average		1.9 ± 0.5 (2σ)	0.244 ± 0.059 (1σ)

a) As reported in Table 3.2

The average value of the branching ratio from 14 observations is 0.244 ± 0.059 where the quoted uncertainty is ±1σ. The kinetic scheme included E-V excitation of the ν_4 bending mode only, because the dipole forbidden ν_2 mode is not expected to participate in the E-V quenching channel. Hess and Moore (97) suggest that the ν_4-ν_2 equilibrium occurs at approximately 10% of the gas kinetic rate, which is more than 50% faster than the total Cl^* quenching process. Consequently the E-V branching ratio determined from ν_4 fluorescence misses the (hidden) ν_2 population that exists in equilibrium with ν_4. This ν_2 population is presumed to have originated in the E-V transfer to ν_4 followed by the rapid

equilibrium with ν_2. Consequently an accurate accounting of the E-V branching ratio must include the equilibrium population in ν_2, which is given by the Boltzmann equation as

$$[\nu_2]_{eq} = [\nu_4]_{eq} \frac{g_2}{g_4} \exp\left(-\left(E_2 - E_4\right)/kT\right) \quad \textbf{(3.34)}$$

where E_2-E_4 is the energy difference between the vibrational levels, 1534 – 1306 = 228 cm^{-1}. The completed calculation for CH_4 at 298K yields $[\nu_2]_{eq} = 1.222\ [\nu_4]_{eq}$ so that the previously stated branching ratio (0.244 ± 0.059) must be increased by the factor 1.222 to 0.30 ± 0.07. This branching ratio is consistent with an absolute Cl^*/CH_4 E-V rate coefficient of (5.7 ± 3.1) x 10^{-12} $cm^3 \cdot molecule^{-1} \cdot s^{-1}$ (2σ).

Combining this E-V branching ratio with the upper limit, ≤ 0.30, for the reactive quenching channel (76) yields a branching ratio bracketed between 0.4 and 0.7 for the remaining E-R,T channel. Interestingly, methane and ozone were outliers in Chichinin's fitting of Cl^* quenching rate coefficients to Equation 1.11 (56). Methane's experimental rate coefficient was 25 times that predicted from the two-parameter fit of a cohort of 18 molecular collision partners presumed to quench Cl^* largely via the E-V excitation channel. Chichinin suggested that the Cl^*/CH_4 E-RT channel might be responsible for the additional measured quenching efficiency beyond that predicted by Equation 1.11. This seems unlikely since roughly a third of the experimental rate can be attributed to the E-V channel whereas Equation 1.11 predicts only a 4% E-V channel. At most, the E-RT

channel is 2.3 times (= 0.70/0.30) more active compared to the E-V excitation channel – but not 25 time greater.

Additionally, it is noted that Chichinin's statement (56) was in error when he claimed that his equation reproduced Dolson and West's Cl^*/SO_2 ν_3/ν_1 branching ratio (89). Rather, the equation more closely predicts the inverse relation. Perhaps one way in which the use of Chichinin's equation might be improved is to account for degeneracies in the sum in Equation 1.11.

E. E-V Branching Ratio Determination for $Cl^*/ CD_4(\nu_4)$

Identical E-V branching ratio measurements were conducted on the $Cl^*/CD_4(\nu_4)$ system as described in the previous section. This ratio can be expressed similarly to equation 3.28:

$$\frac{k_{EV}^*}{k_{EV}^* + k_o^*} = \frac{k_{EV}^*}{k_Q^{CD_4}} \qquad \textbf{(3.35)}$$

As before, k_{EV}^* is the rate coefficient for the $Cl^* \rightarrow CD_4(\nu_4)$ E-V process, k_o^* is the combined rate coefficient for all other $CD_4(\nu_4)$ quenching processes, and $k_Q^{CD_4}$ is the sum of k_{EV}^* and k_o^*, and represents the total $CD_4(\nu_4)$ quenching rate coefficient. The k_{EV}^* rate coefficient in the branching ratio expression is related to the experimentally obtained $CD_4(\nu_4)$ fluorescence intensities by Equations 3.26, 3.27 and 3.36.

$$I_0 = C\left(A \cdot T_\lambda \cdot D_\lambda\right)_{\nu_4} \frac{k_{EV}^{*}\left[CD_4\right]\left[Cl^{*}\right]_0}{\left(k_Q - k_V\right)} \tag{3.36}$$

Here again, the unknown light collection factor, C, is replaced by an equivalent experimental quantity derived from photolytically produced Br^{*} fluorescence and Equation 3.31.

$$C = \frac{I_0^{Br^{*}}}{\left(A \cdot T_\lambda \cdot D_\lambda\right)_{Br^{*}}\left[Br^{*}\right]_0} \tag{3.37}$$

The combined equation for determining k_{EV}^{*} for the Cl^{*}/CD_4 system is given by

$$k_{EV}^{*} = \frac{I_0^{\nu_4}\left(k_{rise} - k_{decay}\right)\left[Br^{*}\right]_0\left(A \cdot T_\lambda \cdot D_\lambda\right)_{Br^{*}}}{I_0^{Br^{*}}\left[CH_4\right]\left[Cl^{*}\right]_0\left(A \cdot T_\lambda \cdot D_\lambda\right)_{CH_4(\nu_4)}} \tag{3.38}$$

The $k_{EV}^{*}/k_Q^{CD_4}$ branching ratio, given by Equation 3.35, is evaluated using experimentally derived values for both rate coefficients. The data for the E-V branching ratio evaluation in the Cl^{*}/CH_4 experiments are tabulated in Tables 3.8 and 3.9.

Table 3.8: Summary of Experimental Data for Cl^*/CD_4 Branching Ratio Calculation

Run #	$[Cl^*]_0$ [a] ($\times 10^{13}$)	$[Br^*]_0$ [a] ($\times 10^{14}$)	$[CD_4]$ [a] ($\times 10^{15}$)	$I_{0(CD_4(\nu_4))}$ [b]	$I_{0(Br^*)}$ [b]	$k_{rise} - k_{decay}$ (10^5 s^{-1})
			Experimental Set #1			
1	4.050	1.614	0.811	0.1792	0.8683	3.453
2	4.050	1.614	1.233	0.1687	0.8683	3.227
3	4.050	1.614	1.233	0.1756	0.8683	2.309
4	4.050	1.614	2.045	0.1900	0.8683	6.588
5	4.050	1.614	2.045	0.1930	0.8683	5.436
6	4.050	1.614	2.434	0.1931	0.8683	6.466
			Experimental Set #2			
1	4.226	1.605	0.422	0.1837	0.7096	0.8708
2	4.226	1.605	0.844	0.1960	0.7096	2.381
3	4.226	1.605	0.844	0.1870	0.7096	1.809
4	4.226	1.605	1.266	0.1985	0.7096	1.401
5	4.226	1.605	1.688	0.2342	0.7096	4.553
6	4.226	1.605	2.110	0.1729	0.7096	3.217
7	4.226	1.605	2.110	0.1840	0.7096	6.853
8	4.226	1.605	2.530	0.2045	0.7096	5.537
			Experimental Set #3			
1	4.239	1.605	0.542	0.1691	0.7821	1.001
2	4.239	1.605	1.074	0.1762	0.7821	2.293
3	4.239	1.605	1.074	0.2385	0.7821	2.026
4	4.239	1.605	1.610	0.1841	0.7821	3.358
5	4.239	1.605	2.142	0.1649	0.7821	4.019
6	4.239	1.605	2.674	0.1801	0.7821	3.551
7	4.239	1.605	2.674	0.2295	0.7821	3.351
8	4.239	1.605	3.210	0.1645	0.7821	6.755
9	4.239	1.605	3.210	0.2466	0.7821	4.858
10	4.239	1.605	3.742	0.1881	0.7821	4.222
11	4.239	1.605	3.742	0.1913	0.7821	3.921
			Experimental Set #4			
1	4.878	1.574	0.587	0.2148	0.7425	1.069
2	4.878	1.574	1.194	0.2628	0.7425	1.622
3	4.878	1.574	1.801	0.2188	0.7425	3.271
4	4.878	1.574	2.408	0.2101	0.7425	3.226
5	4.878	1.574	3.015	0.2036	0.7425	5.245
6	4.878	1.574	3.015	0.2210	0.7425	3.953
7	4.878	1.574	3.622	0.2484	0.7425	3.881

a) Reported in units of molecules/cm^3
b) Reported in units of millivolts (mV)

Table 3.9: Cl^*/CD_4 Branching Ratio Data

Run #	k^*_{EV} (10^{-11} cm^3·molecule^{-1}·s^{-1})	$k^{*\,a}_{Q}$ (10^{-10} cm^3·molecule^{-1}·s^{-1})	Branching Ratio
		Experimental Set #1	
1	6.27	2.6 ± 0.6	0.243
2	2.75	2.6 ± 0.6	0.107
3	3.69	2.6 ± 0.6	0.143
4	4.29	2.6 ± 0.6	0.166
5	5.11	2.6 ± 0.6	0.198
6	4.25	2.6 ± 0.6	0.165
		Experimental Set #2	
1	3.71	2.4 ± 0.6	0.157
2	3.91	2.4 ± 0.6	0.165
3	5.39	2.4 ± 0.6	0.228
4	2.14	2.4 ± 0.6	0.090
5	6.15	2.4 ± 0.6	0.259
6	2.56	2.4 ± 0.6	0.108
7	5.81	2.4 ± 0.6	0.245
8	4.35	2.4 ± 0.6	0.184
		Experimental Set #3	
1	2.73	1.1 ± 0.2	0.255
2	3.93	1.1 ± 0.2	0.367
3	3.29	1.1 ± 0.2	0.307
4	3.36	1.1 ± 0.2	0.314
5	2.71	1.1 ± 0.2	0.253
6	2.51	1.1 ± 0.2	0.235
7	2.09	1.1 ± 0.2	0.195
8	3.27	1.1 ± 0.2	0.305
9	3.03	1.1 ± 0.2	0.283
10	1.75	1.1 ± 0.2	0.164
11	1.86	1.1 ± 0.2	0.174
		Experimental Set #4	
1	3.08	1.2 ± 0.3	0.267
2	2.80	1.2 ± 0.3	0.243
3	3.11	1.2 ± 0.3	0.270
4	2.21	1.2 ± 0.3	0.191
5	2.28	1.2 ± 0.3	0.197
6	2.79	1.2 ± 0.3	0.242
7	2.09	1.2 ± 0.3	0.181
Average		1.4 ± 0.9 (2σ)	0.216 ± 0.065 (1σ)

a) As reported in Table 3.4

An average value of the branching ratio from 32 observations is 0.216 ± 0.065 where the quoted uncertainty is ± 1σ. Here, as in the Cl^*/CH_4 branching ratio experiments, we observe fluorescence only from the asymmetric bend level of CD_4 excited by E-V transfer from Cl^*. Because the V-V equilibrium of the two bending levels is expected to be faster than the E-V kinetics or the subsequent V-T,R relaxation, it is not surprising that we observe no additional time constant for this process in the ν_4 fluorescence. In order to more accurately assess the E-V branching ratio it is necessary to add back that part of the E-V excited ν_4 population that is transferred to the dark ν_2 level in this rapid V-V equilibrium step. Equation 3.34 gives the equilibrium ν_2 population, where E_2-E_4 = 96 cm^{-1}. The completed calculation for CD_4 at 298K yields $[\nu_2]_{eq} = 0.419\ [\nu_4]_{eq}$ so that the previously stated branching ratio (0.216 ± 0.065) must be increased by the factor 1.419 to 0.31 ± 0.09. This branching ratio is consistent with an absolute Cl^*/CD_4 E-V rate coefficient of (4.3 ± 2.6) x 10^{-11} $cm^3 \cdot molecule^{-1} \cdot s^{-1}$ (2σ). It is interesting to note that the E-V branching ratio for Cl^* quenching by CH_4 and CD_4 is ≈30% into the ν_4 bending mode for both methane isotopomers even though the endothermic ΔE values differ four-fold from approximately ½kT (CD_4) to 2kT (CH_4).

Kinetic rate coefficients for Cl^* quenching by CH_4 and CD_4 have been obtained via direct observations of ν_4 bend-excited products, and E-V branching fractions have been determined in these experiments. Theoretical predictions of more probable (faster) Cl^* quenching by CD_4 are fulfilled; however, the expectation of a larger CD_4 branching fraction in the E-V channel is not satisfied. It would be most helpful if some quantum calculations were to be applied to the Cl^*/methanes E-V problem.

F. Suggestions for Further Work

One suggestion for further study is to investigate the enhanced Cl + $CH_4(\nu_4)$ reactivity observed by Bartell and Dolson (96). Similar fluorescence experiments to the ones described in this thesis were performed, with higher methane concentrations and laser pulse energies. A faster initial decay was observed with higher methane and Cl^* concentrations that was not observed at lower concentrations. This observation, if confirmed, is consistent with a second-order loss of $CH_4(\nu_4)$ due to enhanced reactivity with ground-state Cl atoms. Since the amounts of Cl, Cl^* and $CH_4(\nu_4)$ are proportional to the intensity of the laser power, a reaction containing and one of these species would be first-order with respect to the laser power. Similarly, a reaction containing any two of these species would be second-order with respect to the laser power. It would therefore follow that by varying the laser power, the reaction rate under investigation could be determined to be first- or second-order. By accomplishing several of these experiments, the cause of the faster initial decay at higher methane concentrations could be confirmed or refuted to be through a second-order reaction. This topic, vibrationally enhanced reactions, is of current interest; however, other researchers have concentrated on higher vibrational level excitation. The bending mode, which is more difficult to generate via laser methods is readily excited by Cl^* E-V transfer, and possibly also by translational-to-vibrational (T-V) energy transfer.

A second possible avenue for further investigation is to make observations of translational-to-vibrational (T-V) excitation of CH_4/CD_4 with translationally "hot" Cl

atoms or H/D atoms. Hot atoms are defined as those that are intentionally produced to have translational energies much greater than their surroundings at ambient temperatures. It would be of interest to determine if the bending mode of methane could be T-V excited by Cl atoms and then observing the possible accelerated reaction between the bend-excited methane and the relaxed Cl atoms. In their review of "hot atoms" produced by laser photolysis (95), which primarily focused on H/D atoms, Flynn and Weston alluded to preliminary unpublished work with hot Cl atoms in Flynn's group (Columbia University) and cited work in another group (C. B. Moore, UC Berkeley) in which 337 nm photodissociation of Cl_2 produced two Cl atoms with 0.6 eV of translational energy for reaction studies. This same review article showed that the probability and efficiency of T-V energy transfer was enhanced where the Fourier frequency component of the "hot" atom velocity was well matched with a vibrational frequency of its collision partner. These "hot" Cl atoms may provide another mechanism of vibrational excitation in CH_4/CD_4 molecules through an intermolecular collision process. As with the E-V transfer studies undertaken in this thesis work, the future T-V investigations would similarly monitor vibrationally-excited CH_4/CD_4 as the target molecule. This investigation may also test the importance of matching the projectile velocity with the vibrational frequency – a fast H/D atom might excite methane better than a slower and heavier Cl atom.

REFERENCES

(1) Solomon, S. *Rev. Geophys*. **37**, 275-316 (1999) and references cited therein.

(2) Prather, M.; Jaffe, A. H. *J. Geophys. Res.* **95**, 3473-3492 (1990).

(3) Douglass, A. R.; et al. *J. Geophys. Res.* **100**, 13967-13978 (1995).

(4) Santee, M. L.; et al. *J. Geophys. Res.* **101**, 18835-18859 (1996).

(5) Michelson, H. A.; et al. *J. Geophys. Res.* **104**, 26419-26436 (1999).

(6) Oum, K. W.; et al. *Science*. **279**, 74-77 (1998).

(7) Keene, W. C.; Jacob, D. J.; Fan, S.-M. *Atmos. Environ.* **30**, i-iii (1996).

(8) Michelson, H. A. *Acct. Chem. Res.* **34**, 331-337 (2001).

(9) Ravishankara, A. R.; Wine P. H. *J. Chem. Phys*. **72**, 25-30 (1980).

(10) Polanyi, J. C. *J. Quant. Spect. Radiat*. Transf. **3**, 471 (1963).

(11) Callear, A. B. *Ann. Rep. Prog. Chem.* **61**, 48 (1964).

(12) Polanyi, J. C. *Appl. Opt. Suppl.* **2**, 109 (1965).

(13) Callear, A. B. *Appl. Opt. Suppl.* **2**, 145 (1965).

(14) Callear, A. B. *Photochemistry and Reaction Kinetics*. Cambridge University Press, London, Chap. 1 (1967).

(15) Callear, A. B.; Lambert, J. D. *Comp. Chem. Kinetics, Vol. 3*. Elsevier, New York, Chap. 4 (1969).

(16) Cundall, R. B. *Transfer and Storage of Energy by Molecules, Vol. 1*. Wiley-Interscience, New York, Chap. 1 (1969).

(17) Donovan, R. J., Husain, D. *Chem. Rev.* **70**, 489 (1970).

(18) Donovan, R. J., Husain, D. *Adv. Photochem*. **8**, 1 (1971).

(19) McGowan, J. W., ed. *The Excited State in Chemical Physics.* Wiley-Interscience, New York (1975).

(20) Lemont, S.; Flynn, G. W. *Ann. Rev. Chem. Phys*. **28**, 261 (1977).

(21) Houston, P. L. *Photoselective Chemistry*, Part II. Wiley, New York, 381-418 (1981).

(22) Donovan, R. J.; Husain, D.; Stephenson, C. D. *J. Chem. Soc. Faraday Trans*. **66**, 2148 (1970).

(23) Yardley, J. T. *Introduction to Molecular Energy Transfer*. Academic Press, New York (1980).

(24) Ewing, J. J. *Chem. Phys. Lett*. **29**, 50 (1974).

(25) Sharma, R. D.; Brau, C. A. *J. Chem. Phys.* **50**, 924 (1969).

(26) Dillon, T. A.; Stephenson, J. C. *J. Chem. Phys*. **58**, 3849 (1973).

(27) Dillon, T. A.; Stephenson, J. C. *J. Chem. Phys.* **58**, 2056 (1973).

(28) Pritt, A. T.; Coombe, R. D. *J. Chem. Phys*. **65**, 2096 (1976).

(29) Donovan, R. J.; Fotakis, C.; Golde, M. F. *J. Chem. Soc. Faraday Trans. II.* **72**, 2055 (1976).

(30) Gray, C. G. *Can. J. Phys*. **54**, 505 (1976).

(31) Buckingham, A. D. *Disc. Faraday. Soc.* **40**, 232 (1965).

(32) Buckingham, A. D. *Phys. Chem.* **4** (1970).

(33) Nikitin, E. E. *Opt. Spectrosk*. **9**, 16 (1960).

(34) Bjerre, A.; Nikitin, E. E. *Chem. Phys. Lett*. **1**, 179 (1967).

(35) Nikitin, E. E. *Theory of Elementary Atomic and Molecular Processes in Gases*. Oxford University Press, New York (1974).

(36) Bauer, E.; Fisher, E. R.; Gilmore, F. R. *J. Chem. Phys.* **51**, 4173 (1969).

(37) Landau, L. D. *Phys. Z. Sowjet. URSS.* **2**, 46 (1932).

(38) Zener, C. *Proc. Roy. Soc. (London).* **A137**, 696 (1932).

(39) Stuckelberg, E. C. G. *Helv. Phys. Acta.* **5**, 369 (1932).

(40) Karl, G.; Kruus, P.; Polanyi, J. C. *J. Chem. Phys.* **46**, 224 (1967).

(41) Bernstein, R. B.; Levine, R. D. *Chem. Phys. Lett*. **15**, 1 (1972).

(42) Zimmerman, I. H.; George, T. F. *J. Chem. Phys*. **61**, 2468 (1974).

(43) Zimmerman, I. H.; George, T. F. *J. Chem. Soc. Faraday Trans. II*. **71**, 2030 (1975).

(44) Zimmerman, I. H.; George, T. F. *Chem. Phys.* **7**, 323 (1975).

(45) Grimley, A. J.; Houston, P. L. *J. Chem. Phys*. **70**, 4724 (1979).

(46) Park, J.; Lee, Y.; Flynn, G. W. *Chem. Phys. Lett*. **186**, 441 (1991).

(47) Khan, F. A.; Kreutz, T. G.; Flynn, G. W.; Weston, R. E. *J. Chem, Phys.* **92**, 4876 (1990).

(48) Hershberger, J. F.; Hewitt, S. A.; Flynn, G. W. *J. Chem. Phys*. **87**, 1346 (1988).

(49) Haugen, H.; Weitz, E.; Leone, S. R. *J. Chem. Phys*. **83**, 3402 (1985).

(50) Hess, W. P.; Kohler, S. J.; Haugen, H. K.; Leone, S. R. *J. Chem. Phys*. **84**, 2143 (1986).

(51) Hess, W. P.; Leone, S. R. *J. Chem. Phys*. **86**, 3773 (1987).

(52) Tiemann, E.; Kanamori, H.; Hirota, E. *J. Chem. Phys*. **88**, 2457 (1988).

(53) Mashnin, T. S.; Chernyshev, A. V.; Krasnoperov, L. N. *Chem. Phys. Lett*. **207**, 105 (1993).

(54) Dagenais, M.; Johns, J. W. C.; McKellar, A. R. W. *Can. J. Phys.* **54**, 1438, (1976).

(55) Krasnoperov, L. N.; Panfilov, V. N. *Kinetika i Katakiz*. **20**, 540 (1979).

(56) Chichinin, A. I. *J. Chem. Phys*. **112**, 3772 (2000).

(57) Davies, P. B.; Russell, D. K. *Chem. Phys. Lett*. **67**, 440 (1979).

(58) Arepalli, S.; Presser, N.; Robie, D.; Gordon, R. J. *Chem. Phys. Lett.* **118**, 88 (1985).

(59) Urena, A. G., *J. Phys. Chem.* **96**, 8212 (1992).

(60) Crim, F. F., *J. Phys. Chem.* **100**, 12725 (1996).

(61) Moore, C. B.; Smith, I. W. M. *J. Phys. Chem.* **100**, 12848 (1996).

(62) Orr-Ewing, A. J.; Simpson, W. R.; Rakitzis, T. P.; Kandel, S. A.; Zare, R. N. *J. Chem. Phys.* **106**, 5961 (1997).

(63) Lee, S.-H.; Liu, K. *Chem. Phys. Lett*. **290**, 323 (1998).

(64) Lee, S.-H.; Lai, L.-H.; Liu, K.; Chang, H. *J. Chem. Phys.* **110**, 8229 (1999).

(65) Allison, T. C.; Lynch, G. C.; Truhlar, D. G.; Gordon, M. S. *J. Phys. Chem*. **100**, 13575 (1996).

(66) Lee, S.-H.; Liu, K. *J. Chem. Phys.* **111**, 6253 (1999).

(67) Dong, F.; Lee, S.-H.; Liu, K. *J. Chem. Phys.* **115**, 1197 (2001).

(68) Alexander, M. H.; Capecchi, G.; and Werner, H.-J. *Science*, **296**, 715 (2002).

(69) Alexander, M. H.; *et al*., *Phys. Rev. Lett.* **91**, 013201-1 (2003).

(70) Chiltz, G.; Eckling, R.; Goldfinger, P.; Huybrechts, G.; Johnston, H. S.; Meyers, L.; Verbeke, G. *J. Chem. Phys.* **38**, 1053 (1963).

(71) Lin, C. L.; Leu, M. T.; DeMore, W. B. *J. Phys. Chem.* **82**, 1772 (1978).

(72) Zahniser, M. S.; Berquist, B. M.; Kaufman, F. *Int. J. Chem. Kinet*. **10**, 15 (1978).

(73) Dobis, O.; Benson, S. W. *Int. J. Chem. Kinet*. **19**, 691 (1987).

(74) Simpson, W. R.; Orr-Ewing, A. J.; Zare, R. N. *Chem. Phys. Lett*. **212**, 163 (1993).

(75) DeMore, W. B.; Sander, S. P.; Golden, D. M.; Hampson, R. F.; Kurylo, M. J.; Howard, C. J.; Ravishankara, A. R.; Kolb, C. E.; Molina, M. J. In *JPL Publication* 94-26; Jet Propulsion Laboratory: Pasadena, CA, 1994.

(76) Matsumi, Y.; Izumi, K.; Skorokhodov, V.; Kawasaki, M.; Tanaka, N. *J. Phys. Chem A.* **101**, 1216 (1997).

(77) Simpson, W. R.; Rakitzis, T. P.; Kandel, S. A.; Orr-Ewing, A. J.; Zare, R. N. *J. Chem. Phys.* **103**, 7313 (1995).

(78) Simpson, W. R.; Rakitzis, T. P.; Kandel, S. A.; Lev-On, T.; Zare, R. N. *J. Phys. Chem.* **100**, 7938 (1996).

(79) Kandel, S. A.; Zare, R. N. *J. Chem. Phys*. **109**, 9719 (1998).

(80) Hsu, D. S. Y.; Manuccia, T. J. Deuterium Enrichment by CW CO2 Laser Induced Vibrational Photochemistry. In *Advances in Laser Chemistry*; Zewail, A. H., Ed.; Springer-Verlag: Berlin, 1978; pp 89-92.

(81) Hsu, D. S. Y.; Manuccia, T. J. *Appl. Phys. Lett*. **33**, 915 (1978).

(82) Manuccia, T. J.; Hsu, D. S. Y. Deuterium Enrichment by CW Vibrational Photochemistry of Methane-Economic Considerations. In *Laser-Induced Processes in Molecules*; Kompa, K. L., Smith, S. D., Eds.; Springer: Heidelberg, 1979; pp 270-271.

(83) Vijin, V. V.; Mikheev, A. N.; Petrov, A. K.; Molin, Y. N. *React. Kinet. Catal. Lett.* **3**, 79 (1975).

(84) Chesnokov, E. N.; Strunin, V. P.; Serdyuk, N. K.; Panfilov, V. N. *React. Kinet. Catal. Lett*. **3**, 131 (1975).

(85) Kim, Z. H.; Alexander, A. J.; Bechtel, H. A.; Zare, R. N. *J. Chem. Phys*. **115**, 179 (2001).

(86) Atkinson, R.; Baulch, D. L.; Cox, R. A.; Hampson, J. R. F.; Kerr, J. A.; Rossi, M. J.; Troe, J. A. *J. Phys. Chem. Ref. Data* **28**, 191 (1999).

(87) Chichinin, A. I. *J. Phys. Chem. Ref. Data*. **35**, 869 (2006).

(88) Huber, K. P.; Hertzberg, G. "Molecular Spectra and Molecular Structure"; Van Nostrand Reinhold, New York, 1979; Vol. 4 "Constants of Diatomic Molecules".

(89) Dolson, D. A.; West, D. S. *Chem. Phys. Lett*. **216**, 258 (1993).

(90) Sotnichenko, S. A.; Vokun, V. Ch.; Nadkhin, A. I. Chem. Phys. Lett. **153**, 560 (1988).

(91) Bartell, C. A.; Dolson, D. A. *Abstr. Pap. Am. Chem. Soc.* **208**, 287-Phys. Part 2 (1994).

(92) Chichinin, A. I.; Sotnichenko, S. A.; Krasnoperov, L. N. *Chem. Phys. Lett*. **138**, 371 (1987).

(94) Herzberg, G. *Infrared and Raman Spectra of Polyatomic Molecules* (Van Nostrand, Toronto, 1966), Vol. 2.

(95) Flynn, G. W.; Weston, Jr., R. E. *Ann. Rev. Phys. Chem*. **37**, 551 (1986).

(96) Hess, P., Moore, C. B. *J. Chem. Phys*. **65**, 2339 (1976).

(97) Hess, P., Moore, C. B. *J. Chem. Phys*. **72**, 5525 (1980).

(98) Brumfield, Brian, M.S. Thesis, Wright State University, 2005.

(99) Gribov, L. A.; Smirnov, V. N. *Sov. Phys. Usp.* **4,** 919 (1962).

(100) Sverdlov, L. M.; Kovner, M. A.; Krainov, E. P. *Vibrational Spectra of Polyatomic Molecules*. John Wiley & Sons, New York (1974). (English translation)